



HAL
open science

PAX3 Confers Functional Heterogeneity in Skeletal Muscle Stem Cell Responses to Environmental Stress

Audrey Der Vartanian, Marie Quéting, Stéphanie Michineau, Frédéric Auradé, Shinichiro Hayashi, Christelle Dubois, Didier Rocancourt, Bernadette Drayton-Libotte, Anikó Szegedi, Margaret Buckingham, et al.

► **To cite this version:**

Audrey Der Vartanian, Marie Quéting, Stéphanie Michineau, Frédéric Auradé, Shinichiro Hayashi, et al.. PAX3 Confers Functional Heterogeneity in Skeletal Muscle Stem Cell Responses to Environmental Stress. *Cell Stem Cell*, 2019, 24 (6), pp.958-973.e9. 10.1016/j.stem.2019.03.019 . hal-03082589

HAL Id: hal-03082589

<https://hal.science/hal-03082589>

Submitted on 25 Oct 2021

HAL is a multi-disciplinary open access archive for the deposit and dissemination of scientific research documents, whether they are published or not. The documents may come from teaching and research institutions in France or abroad, or from public or private research centers.

L'archive ouverte pluridisciplinaire **HAL**, est destinée au dépôt et à la diffusion de documents scientifiques de niveau recherche, publiés ou non, émanant des établissements d'enseignement et de recherche français ou étrangers, des laboratoires publics ou privés.



Distributed under a Creative Commons Attribution - NonCommercial 4.0 International License

PAX3 confers functional heterogeneity in skeletal muscle stem cell responses to environmental stress

Audrey Der Vartanian^{1,2}, Marie Quétin^{1,2}, Stéphanie Michineau^{1,2}, Frédéric Auradé^{1,3}, Shinichiro Hayashi⁴, Christelle Dubois^{1,2}, Didier Rocancourt⁵, Bernadette Drayton-Libotte^{1,2}, Anikó Szegedi^{1,2}, Margaret Buckingham⁵, Simon J. Conway⁶, Marianne Gervais^{1,2,*}, Frédéric Relaix^{1,2,7,8,9,10,11*}

*: senior author

¹Inserm, IMRB U955-E10, 94000, Créteil, France

²Faculté de Médecine, Université Paris Est Créteil, 94000, Créteil, France

³Sorbonne Université, Inserm U974, Center for Research in Myology, Paris, France

⁴Department of Neuromuscular Research, National Institute of Neuroscience, National Center of Neurology and Psychiatry, 187-8551, Tokyo, Japan

⁵Department of Developmental and Stem Cell Biology, Centre National de la Recherche Scientifique, Unité de Recherche Associée 578, Institut Pasteur Paris

⁶Herman B Wells Center for Pediatric Research, Indiana University School of Medicine, Indianapolis, IN, 46202, USA

⁷Ecole Nationale Vétérinaire d'Alfort, 94700, Maisons-Alfort, France

⁸Etablissement Français du Sang, 94017, Créteil, France

⁹APHP, Hopital Henri Mondor, DHU Pepsy & Centre de Référence des Maladies Neuromusculaires GNMH, 94000, Créteil, France

¹⁰Lead Contact

¹¹Correspondence: frederic.relaix@inserm.fr

SUMMARY

Muscle satellite cells (MuSCs) are the quiescent muscle stem cells required for adult skeletal muscle repair. The impact of environmental stress such as pollution on MuSC behavior remains unexplored. We evaluated the impact of 2,3,7,8-tetrachlorodibenzo-p-dioxin (TCDD) exposure, a ubiquitous and highly toxic pollutant, on MuSCs by combining *in vivo* mouse molecular genetic models with *ex vivo* studies. While all MuSCs express the transcription factor PAX7, we show that a subset also express PAX3 and exhibit resistance to environmental stress. Upon systemic TCDD treatment, PAX3-negative MuSCs display impaired survival, atypical activation and sporadic differentiation through xenobiotic Aryl Hydrocarbon Receptor signaling. We further show that PAX3-positive MuSCs become sensitized to environmental stress when PAX3 function is impaired and that PAX3-mediated induction of mTORC1 is required for protection. Our study therefore identifies a functional heterogeneity of MuSCs in response to environmental stress controlled by PAX3.

INTRODUCTION

Adult stem cells are found in many mammalian tissues where they are involved in tissue maintenance, repair and regeneration *via* self-renewal and differentiation of tissue-specific cell types (Weissman, 2000). Skeletal muscle satellite cells (MuSCs) are the myogenic stem cells of adult muscle embedded between the plasmalemma and basal lamina of myofibers (Katz, 1961; Mauro, 1961). Under normal homeostatic conditions, MuSCs are in a quiescent state G0 (Cheung and Rando, 2013) and are characterized by the expression of PAX7, a key transcription factor required for their maintenance (Horst et al., 2006; Lepper and Fan, 2010; Oustanina et al., 2004; Relaix, 2006; Seale et al., 2000). PAX3, a paralogue of PAX7 has also been detected in a subset of adult MuSCs (Calhabeu et al., 2013; Relaix et al., 2006). Upon trauma or in diseased conditions, PAX7+ MuSCs in G0 will be activated, enter cell cycle G1, express the myogenic factor MYOD, undergo extensive expansion and differentiate into myogenic cells by downregulating PAX7 and inducing MYOGENIN with the expression of other downstream myogenic-specific genes, allowing tissue repair (Bismuth and Relaix, 2010; Olguin and Pisconti, 2012; Zammit et al., 2006). A subset will downregulate MYOD and exit the cell cycle to self-renew the pool of PAX7+ MuSCs for future needs (Collins, 2006; Zammit et al., 2004). Interestingly, distant injury can prime G0 PAX7+ MuSCs for activation in an intermediate G(alert) state characterized by cell size increase and PI3K-mTORC1 activation, but without disrupting the niche nor entering the cell cycle or myogenesis (Rodgers et al., 2014). Alterations of the balance between quiescence, activation and differentiation may result in impaired function, premature MuSCs exhaustion and subsequent skeletal muscle regeneration failure.

Despite the fact that environmental pollutants are a part of modern life, the impact of environmental stress on adult stem cells remains poorly understood. It has been suggested that environmental pollutants could exert their adverse effect by targeting stem cell function, resulting in changes in the stem cell differentiation potential and alterations of self-renewal capacity (Bock, 2017). Recent studies redefining the cell identity of quiescent and early activated MuSCs (Machado et al., 2017; van den Brink et al., 2017; van Velthoven et al., 2017) using direct approaches such as *in situ* fixation (Machado et al., 2017) show that the Aryl Hydrocarbon Receptor (AHR) is highly expressed in quiescent and early activated MuSCs, suggesting these stem cells are highly responsive to environmental stress. AHR is a cytosolic ligand-activated transcription factor that mediates toxic effects of pollutants such as 2,3,7,8-tetrachlorodibenzo-*p*-dioxin (TCDD) in vertebrates (Okey, 2007). Following ligand activation, the AHR-ligand complex translocates into the nucleus and heterodimerizes with the AHR nuclear translocator (ARNT) to induce expression of detoxification pathways, including those coding for the phase I xenobiotic-metabolizing cytochrome P450 enzymes such as CYP1A1 (Carrier et al., 1994; Ma, 2001). TCDD is the most toxic and ubiquitous persistent organic pollutants to which humans are daily exposed (Parzefall, 2002). The chemical structure of these pollutants allows them to be soluble in lipids leading to their facilitated bioaccumulation in adipose tissue (Pavlikova et al., 2015).

Here we identify a bimodal response of MuSCs to systemic environmental stress exposure depending on the expression of PAX3. We show that injection of TCDD promotes, without

local injury, AHR-dependent loss of PAX3 negative MuSCs by activation and fusion, and, for a small subset, impaired survival. Interestingly, PAX3-expressing MuSCs are protected *via* induction of G(alert) features. This resistance is dependent on PAX3 function *in vivo* and can be reversed by impairing mTORC1 function. Our study therefore reveals that MuSCs display a functional heterogeneity in responding to environmental stress depending on PAX3 function.

RESULTS

Exposure to TCDD pollutant affects skeletal homeostasis and the MuSC pool.

To evaluate the impact of environmental stress on skeletal muscle, wild-type mice were injected intraperitoneally with 4µg/kg of 2,3,7,8-tetrachlorodibenzo-*p*-dioxin (TCDD) twice per week for one month (**Figure 1A**). Several muscles were collected for histological analysis (**Figure 1A-E**). TCDD treatment had no impact on fat deposition and fibrosis in both TA and biceps (**data not shown**). However, histological analysis revealed significant expression of the embryonic isoform of myosin heavy chain (eMHC) in both muscles following systemic TCDD exposure, suggesting ongoing contribution from MuSCs to myofibers (**Figure 1B**). Interestingly, the percentage of eMHC+ myofibers upon TCDD treatment was significantly higher in TA than in biceps (**Figure 1C**). Since MuSCs are mediating muscle regeneration, we tested whether exposure to TCDD may affect their number. Quantification of PAX7+ MuSCs revealed a substantial reduction in all muscles examined. Consistent with eMHC analysis (**Figure 1B**), reduction in PAX7+ cell number was more pronounced in hindlimb muscles (EDL and TA) than in trunk and forelimb muscles (biceps and diaphragm) (**Figure 1D-E**). Thus, TCDD-induced systemic environmental stress triggers sporadic and muscle-specific loss of PAX7+ MuSCs associated with a regenerative phenotype in the absence of local damage.

Differential loss of MuSCs exposed to TCDD correlates with muscle-specific expression of PAX3.

MuSCs are heterogeneous regarding PAX3 expression (Calhabeu et al., 2013; Kuang et al., 2006; Relaix et al., 2006) suggesting a possible link with the muscle-specific impact of environmental stress. Using a *Pax3*^{nlacZ-IRESGFP/+} knock-in mouse line that express a dual β-Galactosidase and GFP reporter (**Figure 2A**), we first characterized the pattern of PAX3 expression in various adult muscles. Biceps and diaphragm showed the strongest X-gal (PAX3) staining, whereas moderate expression was observed in pectoralis, abdominal, TA and EDL muscle staining (**Figure 2B**). Plantaris, quadriceps, soleus and gastrocnemius showed only rare sporadic X-gal staining (**Figure 2B**). As a whole, PAX3 is highly expressed in trunk and forelimb MuSCs and low in most hindlimb muscles. In order to show that *Pax3* reporters faithfully reproduced PAX3 expression *in vivo* we intercrossed *Pax7*^{creERT2/+} (Murphy et al., 2011) with *Pax3*^{GFP/+} (Relaix et al., 2005) and *Pax3*^{flox/+} mice (Koushik et al., 2002)(**Figure 2C**). PAX3 protein expression was detected in GFP+ MuSCs from both isolated biceps myofibers and plated PAX7+ GFP+ MuSCs from control (*Pax3* Ctrl) mice (**Figure 2D-E**). We did not observe any PAX3 expression elsewhere in skeletal muscle (Alonso-Martin et al., 2018). This specific PAX3 expression was lost in GFP-traced cells from *Pax7*^{creERT2/+}:

Pax3^{GFP/flox} (Pax3 cKO) mice (**Figure 2D-E**). Thus PAX3 is expressed in a muscle-specific stem cells subpopulation.

We next investigated the impact of TCDD exposure on PAX3+ (expressing both PAX7 and PAX3) and PAX3- (expressing only PAX7) MuSCs using *Pax3*^{GFP} expression in TA and biceps (**Figures 2F-G, S1**). PAX3+ MuSCs were revealed on muscle section by co-immunostaining using anti-GFP (PAX3) and anti-PAX7 antibodies (**Figure S1**). At 10 weeks (end of the 4 weeks treatment), in control mice, only a few TA MuSCs (14%) expressed PAX3 whereas in the biceps, the majority (55%) of the PAX7-expressing cells were also PAX3 positive (**Figures 2F-G, S1B**). Strikingly, systemic TCDD exposure specifically decreased the PAX3- MuSC subpopulation in both TA and biceps whereas PAX3+ MuSCs were not affected (**Figures 2F-G, S1B**). Thus, TCDD exposure induced a specific loss of PAX3- MuSCs in adult skeletal muscle, while PAX3+ MuSCs are preserved (**Figures 2G, S1B**). Long-term studies indicated that the specific loss of MuSCs persisted 8 weeks after TCDD treatment withdrawal (**Figures 2F-G, S1C**).

Bimodal response of MuSCs to TCDD correlates with PAX3 expression.

In order to further characterize the impact of TCDD exposure on MuSC subpopulations, we analyzed the activation and differentiation status of both PAX3+ and PAX3- MuSCs on freshly isolated myofibers (T0h) (**Figure 3A-C**). In vehicle-exposed *Pax3*^{GFP/+} mice, all MuSCs along the myofibers expressed PAX7, but showed no sign of activation/differentiation, demonstrating that all MuSCs, independently of PAX3 expression, were quiescent (**Figure 3B-C**). In contrast, TCDD exposure promoted a significant activation of PAX3- MuSCs, detected by the co-expression of PAX7 and MYOD, while GFP+ (PAX3+) MuSCs remained mostly quiescent (**Figure 3B-C**). Interestingly, under TCDD exposure a small population of cells maintaining under the basal lamina expressed only MYOD (**Figure 3B** shown with an asterisk). This PAX7-MYOD+ cell population was negative for GFP expression (PAX3-subpopulation). In addition, we also observed that upon TCDD treatment, a few cells located under the basal lamina expressed MYOG and was detected in a GFP- subpopulation at the end of the treatment (10 weeks), then declines 4 weeks post-treatment (14 weeks) and becomes barely detectable at 8 weeks post-treatment (18 weeks) (**Figure 3D-F**). Similar results were obtained on freshly isolated MuSCs (**Figure S2A-C**). We conclude that TCDD exposure induces a specific activation and differentiation of PAX3- MuSCs.

As PAX3 and PAX7 are also involved in cell survival (Borycki et al., 1999; Relaix et al., 2006; Relaix et al., 2003), we analyzed apoptosis and necrosis by flow cytometry using Sytox/Annexin V staining. We isolated GFP- expressing cells from *Pax3*^{GFP/+} adult forelimbs and *Tg:Pax7nGFP* (Sambasivan et al., 2009) hindlimb muscles treated with TCDD (**Figures 3G-H, S2D-E**). Since PAX7+ cells were isolated from hindlimb muscles, the vast majority of the analyzed MuSCs are not expressing PAX3 (PAX3-, see **Figure 2B**). In vehicle-treated mice, PAX3- and PAX3+ cells present a similar profile regarding the percentage of living, early apoptotic, apoptotic and necrotic cells (**Figures 3H, S2E**). Interestingly, TCDD exposure triggers a specific cell death of the PAX3- MuSCs in adult muscles (**Figure S2E**, red circle), whereas the PAX3+ MuSC subpopulation was not overtly affected (**Figures 3H, S2E**). Thus, TCDD exposure triggers a specific loss of PAX3- MuSCs through atypical activation and impaired survival.

TCDD induces fusion of PAX3- MuSCs to myofibers without local injury.

In order to further analyze the behavior of activated MYOD+ MuSCs upon TCDD exposure *in vivo*, we generated a *Tg:MyoD-nLacZ* transgenic mouse model using a 230kb BAC that contains all the reported regulatory elements of *MyoD* linked to a *nLacZ* reporter (*Tg:BAC MyoD-nLacZ*, **Figure 4A**). We performed systemic TCDD exposure in *Tg:MyoD-nLacZ* mice and analyzed β -Galactosidase (β -Gal) expression in TA and biceps (**Figure 4B**). The stability of the nLacZ protein allowed us to follow MYOD-derived myogenic cells and their contribution to myofibers (resulting from myoblast cell fusion) using an anti- β -Gal antibody (**Figures 4C-F**). Co-immunostaining experiments using a PAX7 antibody revealed that in vehicle-treated mice the vast majority of the MuSCs in both TA and biceps did not co-express β -Gal (**Figure 4C, 4E**). Systemic TCDD treatment promoted activation of MuSCs by reducing the proportion of quiescent PAX7+MYOD- cells in both TA and biceps *in vivo* (**Figure 4C-D**), increasing the proportion of activated PAX7+ cells co-expressing MYOD in both TA and biceps (**Figure 4C, 4E**), consistent with our previous findings on freshly isolated myofibers (**Figure 3B-C**). This effect was more pronounced in TA, which contains a very low number of PAX3+ MuSCs compared to the biceps (**Figures 4C, 4E, 2B, 2G**). This muscle-specific MuSC activation linked with PAX3 expression also translated into an increased number of β -Gal+ myofibers (**Figures 4C, asterisks and 4F for quantifications**) in the TA compared with biceps. To validate the differential myofiber contribution between PAX3+ and PAX3- MuSCs, we performed lineage studies by intercrossing *Pax3*^{GFP/+}, *Pax7*^{CreERT2/+} and *R26*^{stop-Tomato} mice, relying on the stability of the GFP to trace Pax3GFP MuSCs and the expression of Tomato upon tamoxifen treatment to follow all MuSCs (**Figure 4G**). Cre expression was induced using 10 days of tamoxifen diet in adult *Pax3*^{GFP/+}; *Pax7*^{CreERT2/+}; *R26*^{stop-Tomato} mice prior to TCDD treatment (**Figure 4G**). In vehicle-treated mice, we observed a low and similar level of fusion of GFP+ and GFP- MuSCs over the 4 weeks periods of treatment, likely originating from a low homeostatic turn-over of MuSCs (**Figure 4H-J**), as previously observed (Pawlikowski et al., 2015). By contrast, upon TCDD treatment, while the GFP+ MuSCs did not show increased contribution to myofibers, GFP- MuSCs significantly increased their fusion with myofibers (**Figure 4H-J**). We next examined the percentage of centrally located nuclei in myofibers in both TA and biceps at the end of TCDD treatment (10 weeks) and, 4 and 8 weeks after TCDD treatment withdrawal (**Figure 4K-L**). We observed a drastic increase in centronucleated myofibers of mice exposed to TCDD 4 weeks after treatment withdrawal (14 weeks), with a higher percentage in TA compared to biceps (**Figure 4K-L**). This effect was still observed 2 months post-treatment (18 weeks), albeit at lower levels, suggesting a progressive return to normal homeostasis after TCDD withdrawal (**Figure 4K-L**). These results demonstrated that TCDD induces the specific activation and long-term contribution of PAX3- MuSCs into myofibers.

AHR signaling is required for MuSC activation in response to TCDD.

In many cell types, the effect of pollutants such as TCDD is mediated by the Aryl Hydrocarbon Receptor (AHR) pathway (Marlowe and Puga, 2005). To evaluate the involvement of AHR signaling in MuSCs from mice exposed to TCDD we generated a MuSC-specific AHR conditional knock-out mouse model (*Pax7*^{CreERT2/+}; *AHR*^{fl/fl}) (AHR cKO) (**Figure 5A**). We validated the efficiency of AHR deletion following tamoxifen-induced Cre ablation in AHR cKO MuSCs compared to AHR control MuSCs (**Figure S3A-D**). We also evaluated the

activation of the AHR pathway in MuSCs isolated from mice exposed to TCDD by quantifying the AHR target genes, such as *Cyp1a1*, *AHRR*, *Nqo1*, *Cyp1a2* and *Cyp1b1* (**Figures 5B, S3D**). As anticipated, canonical AHR downstream genes were significantly increased in mice treated with TCDD compared to vehicle-treated controls while this effect was abrogated in AHR cKO mice (**Figures 5B, S3D**). Interestingly, *Pax3* gene expression was significantly increased under TCDD treatment. This effect was blunted in AHR cKO mice, suggesting that PAX3 expression is downstream of AHR signaling (**Figure 5B**). We also observed an AHR-dependent increase in MYOD expression in MuSCs isolated from mice treated with TCDD (**Figure 5B**), in keeping with our histological analysis demonstrating that TCDD induces the activation of PAX3- MuSCs (**Figures 3A-F, 4A-E**). We next explored whether the loss of quiescence induced by TCDD treatment in MuSCs is mediated by AHR signaling. While a significant subset of MuSCs was displaying signs of atypical activation (either PAX7+MYOD+KI67- or PAX7-MYOD+KI67+) in TCDD-treated mice, we observed a complete abrogation of this activation in AHR cKO mice (**Figure 5C-D, S3E-G**). We conclude that TCDD promotes aberrant activation of PAX3- MuSCs *via* AHR signaling.

Impairing PAX3 expression leads to MuSCs sensitization to TCDD.

We then analyzed whether PAX3 expression is required for the protective effect from TCDD in PAX3+ MuSCs. To this end, we compared Pax3 control mice to Pax3 cKO in which PAX3-ablated cells are labeled with GFP (GFP+) (**Figures 6A, S4, 2C-2E**). We first checked that *Pax3* was efficiently downregulated in MuSCs of Pax3 cKO mice (**Figure 6B**). We next analyzed the impact of TCDD treatment for the expression of canonical AHR signaling target genes, in both GFP+ and GFP- MuSC subpopulations isolated from Pax3 Ctrl or Pax3 cKO mice (**Figures 6B, S4B**). While *Cyp1a1*, *Nqo1*, *Cyp1a2* and *Cyp1b1* (**Figures 6B, S4B**) were highly induced upon TCDD exposure in both GFP+ and GFP- MuSC subpopulations of Pax3 Ctrl mice, *AHRR* displayed a differential response linked with PAX3 expression (**Figure 6B**). In Pax3 Ctrl mice, GFP+ MuSCs displayed enhanced activation of the AHR signaling pathway targets (**Figures 6B, S4B**) upon TCDD treatment compared to GFP- MuSCs. Ablation of PAX3 in GFP+ MuSCs abrogated the enhanced TCDD-induced AHR activation (**Figures 6B, S4B**). Upon TCDD exposure, *MyoD* expression was specifically induced in GFP+ MuSCs lacking PAX3 (Pax3 cKO mice) suggesting that PAX3 function is required to shield GFP+ MuSCs from the impact of TCDD (**Figure 6B**).

In order to establish that PAX3 function is required for PAX3+ MuSC resistance to environmental stress, we treated Pax3 Ctrl and Pax3 cKO mice with TCDD and analyzed the behavior of GFP+ MuSCs (**Figures 6C and 6D**). We found that while GFP+ MuSCs remain quiescent (PAX7+MYOD-) in control mice treated with TCDD, PAX3-defective GFP+ MuSCs displayed a significant increase in activation (PAX7+MYOD+) (**Figures 6C and 6D**). Our result highlights a protective role of PAX3 against the activation of adult MuSCs by environmental pollutants.

We next investigated the link between AHR and PAX3 in *Pax3*^{GFP/+} mice (**Figures 6E, S4C**). On vehicle-treated biceps, PAX3 and AHR co-immunostaining revealed that AHR was mainly expressed in the cytoplasm of both PAX3- and PAX3+ MuSCs (**Figures 6F-G, S4D**). Under TCDD treatment, both subpopulations presented a nuclear localization of AHR with a higher staining intensity in the PAX3+ subpopulation (**Figures 6F-G, S4D**), suggesting that activation

of the AHR pathway is exacerbated after TCDD exposure in the PAX3⁺ subpopulation (**Figures 6B, 6F-G, S4**). Our data therefore demonstrate that PAX3 expression is linked with an enhanced stimulation of the AHR pathway and PAX3 function is required to protect MuSCs from the effects of TCDD exposure.

PAX3 expression controls the adaptive transition of quiescent MuSCs through the mTORC1 pathway under environmental stress.

In the course of our study, we noticed that PAX3⁺ MuSCs treated with TCDD displayed a significantly increased cell size compared to controls (**Figure S2B**). To validate this observation, we quantified the size of freshly isolated PAX3⁺ (GFP⁺) and PAX3⁻ (GFP⁻) MuSCs using *Pax3*^{GFP/+} mice treated with TCDD and compared to the control condition 2h post-plating. We found that PAX3⁺ MuSCs displayed an increased cell size compared to PAX3⁻ MuSCs (**Figures 7A-B, S2B**). The cell size of PAX3⁺ MuSCs was further significantly increased upon systemic TCDD treatment whereas PAX3⁻ MuSC size remained constant (**Figures 7B, S5A-D**). Since we observed that TCDD exposure promotes PAX3⁺ cell size increase in the absence of activation or local injury disrupting the MuSC niche, we hypothesized the potential involvement of the mTORC1 pathway in the protection of PAX3⁺ MuSCs against environmental stress, similarly to the G0/G(alert) transition (Rodgers et al., 2014). We combined GFP and antibodies-based cell sorting to evaluate EdU incorporation after a 4h chase on freshly sorted cells. We analyzed the first division profiling of isolated PAX3⁺ and PAX3⁻ MuSCs (**Figures 7A-B, S5F**). As previously demonstrated in activated cells (Rodgers et al., 2014), PAX3⁻ MuSCs exposed to TCDD presented the highest EdU incorporation at 12, 24 and 48h (**Figures 7B, S5F**). Significant EdU incorporation was also observed in PAX3⁺ MuSCs following TCDD treatment compared to the control condition (**Figures 7B, S5G**). We then determined the ratio of mtDNA content in both MuSC subpopulations. Compared to controls, mtDNA content strongly increased in PAX3⁻ MuSCs under TCDD exposure, confirming their activation state whereas PAX3⁺ MuSCs showed lower but still significant increase in mtDNA level, suggesting the enhanced mitochondrial activity of PAX3⁺ MuSCs upon TCDD exposure (**Figure 7D**). Taken together these results suggest that PAX3⁺ MuSCs exposed to TCDD have different cell cycle kinetics and display features of 'alerted' MuSCs (Rodgers et al., 2014). We accordingly analyzed phosphorylation of S6 ribosomal protein (p-S6), a signature of mTORC1 signaling, in PAX3⁺ and PAX3⁻ MuSCs treated with TCDD in both Pax3 Ctrl and Pax3 cKO mice. In vehicle-treated MuSCs, only sporadic staining for p-S6 was observed (**Figures 7E-F, S5H**). Strikingly, in TCDD-treated Pax3 Ctrl mice, nearly all GFP⁺ MuSCs were p-S6 positive upon TCDD treatment, whereas p-S6 was not seen in GFP⁻ MuSCs (**Figures 7F, S5H**). This staining was lost in Pax3 cKO mice (**Figures 7F, S5H**), demonstrating that TCDD exposure triggers PAX3-dependent activation of the mTORC1 pathway. We observed that the p-S6 positive staining declined by 50% in PAX3⁺ MuSCs one month after the end of the TCDD withdrawal and was no longer detected after two months post-treatment (**Figures 7E-F**). To determine whether mTORC1 signaling is mediating PAX3⁺ MuSCs protection against TCDD, we isolated biceps myofibers from Pax3 Ctrl and Pax3 cKO mice and used rapamycin, an mTORC1 inhibitor (**Figure 7G-I**). We first verified that 15h of rapamycin treatment was impairing S6 phosphorylation using GFP, PAX7 and p-S6 immunostaining (**Figure 7H-I**). We next assayed the myogenic status of TCDD-exposed control and Pax3 cKO MuSCs (**Figure 7H-I**). Importantly, we observed that PAX3⁺ MuSCs treated with rapamycin became sensitized to TCDD treatment and showed similar levels of

MYOD activation compared to PAX3⁻ MuSCs (**Figure 7J-K**). In all experiments, PAX3 cKO MuSCs had an inactive mTORC1 pathway. Our results therefore demonstrate that PAX3 controls the adaptive response of MuSCs *via* the mTORC1 signaling pathway.

DISCUSSION

In contrast to PAX3⁻ cells, PAX3⁺ MuSCs exposed to TCDD display cellular features previously identified in a G0 to G(alert) transition state (increase in cellular size, priming for activation, elevated mitochondrial activity). This G(alert) cell response was first reported in hindlimb muscles contralateral to the site of muscle injury (Rodgers et al., 2014). Following injury, tissue damage led to activation of circulating Hepatocyte growth factor Activator (HGFA) that catalyzes the proteolytic processing of pro-HGF into active HGF in tissues throughout the body. This signal stimulates an injury-induced transition of MuSCs into G(alert) in uninjured muscles, improving their capacity to repair damaged tissues (Rodgers et al., 2017). Our study demonstrates that TCDD reproduces the main feature of HGFA release and induces the transition of PAX3⁺ MuSCs into a G(alert)-like state, but without injury and by a systemic mechanism. In addition, Lee et al. also reported that HMGB1 administration enhances tissue repair *via* induction of the Galert response (Lee et al., 2018). Our observation leads to a conceptual questioning of the potential stress nature of the systemic signals following injury. In fact, it would be interesting to determine if other stem cell systems may show a specific response to limit the impact of environmental stress and whether PAX3 might also be regulating other forms of stress in muscle stem cells. This would be consistent with a study demonstrating that PAX3 is required for radiotolerance of MuSCs (Scaramozza et al., 2019).

Recent studies have shown that MuSC activation following dissociation is a fast (2-3h) process (van den Brink *et al.*, 2017; Machado *et al.*, 2017; van Velthoven *et al.*, 2017) that also involves mTORC1 signaling (Wang et al., 2018). This is in sharp contrast to the time required for the first division (24h to 48h, see **Figure 7B**). Upon environmental stress, PAX3⁻ MuSCs may have exited quiescence with a transitory increase in mTORC1 signaling, but the activation of the pathway might not be maintained when activated cells enter the myogenic program (**Figure 7E-F**). On the other hand, the higher resistance of PAX3⁺ MuSCs to an environmental stress stimulus might maintain them in this transitory mTORC1 state, associated with sustained p-S6 signal. This would be consistent with our long-term analysis demonstrating that p-S6 staining in PAX3⁺ MuSCs is progressively lost after TCDD withdrawal (**Figure 7E-F**).

We show that the impact of TCDD on PAX3⁻ MuSCs is mediated by AHR signaling, implying a potential role of AHR in muscle stem cell physiology. Surprisingly, PAX3⁺ MuSCs present a higher AHR activation upon TCDD without any consequence for their number, or activation. The role of the AHR pathway has previously been evaluated in other stem cells, but bimodal responses were not reported. Exposure of mice to TCDD and prolonged activation of AHR in hematopoietic stem cells lead to an impairment in progenitor population number and quiescence (Singh et al., 2009) without stromal niche alteration. In addition, AHR was shown to modulate mitotic progression and loss of pluripotency in embryonic stem cells (Ko et al., 2016). The differential level of AHR activation, observed in both basal and TCDD conditions,

could be linked to the expression of *AHRR* that is significantly increased in PAX3⁺ MuSCs. PAX3 might therefore reduce the feedback loop regulation of the AHR pathway through the direct or indirect repression of AHRR. Our results suggest that PAX3 may thus be involved in the fine tuning of the AHR pathway output.

Heterogeneity among MuSCs has been previously shown, depending on their asymmetric self-renewal and commitment ability marked by *Myf5*-driven Cre activity (Kuang et al., 2007), their division rate (Chakkalakal et al., 2012) or PAX7 expression levels (Rocheteau et al., 2012). Our study reveals that the expression of the transcription factor PAX3 determines a functional heterogeneity within the MuSC pool in response to an environmental insult. We have examined the muscle-specific expression of PAX3 in MuSCs and found it conserved during aging and without significant variations between animals (data not shown), suggesting a tight control of its expression. It has been proposed that use of alternative polyA signals coupled with miRNA regulation is regulating Pax3 expression (Boutet et al., 2012). The PAX3 protein is also subjected to post-translational modifications (Boutet et al., 2007). The complex regulatory control of *Pax3* expression is consistent with the importance of maintaining clonal complexity of MuSCs during aging (Tierney et al., 2018).

One can speculate that the heterogeneity of MuSCs regarding the expression of PAX3 might be linked with evolutionary pressure on PAX3 function under environmental stress. For example, maintaining the PAX3⁻ MuSC subpopulation in hindlimb muscles, highly solicited for locomotion and exposed to injuries, would ensure rapid regeneration of these muscles to despite the risk of compromising the self-renewal of MuSCs over time. In contrast, muscles responsible for vital functions such as respiration (trunk and diaphragm muscles) or prehension (forelimb muscles), which may be more directly in contact with pollutants, can explain the selection in these muscles of a greater PAX3⁺ MuSC subpopulation presenting a resistance to environmental stress.

Activation of satellite cells is the critical step in the initiation of muscle homeostasis or regeneration. It is subjected to multiple layers of tight regulation mainly mediated by various signaling pathways (Bentzinger et al., 2013) interacting with myogenic regulatory factors such as MYOD (Smith et al., 1994). After activation, MYOD is involved in proliferation of MuSCs (Megeny et al., 1996). We show that, upon TCDD exposure, PAX3⁻ MuSCs display survival impairment, aberrant activation, proliferation and sporadic abnormal contribution to myofibers demonstrated by the presence of eMHC⁺ fibers. This behavior is highly unusual for an uninjured muscle without apparent damage of the stem cell niche that maintains MuSCs quiescent *via* Notch signaling (Bjornson et al., 2012; Mourikis et al., 2012) and local synthesis of Collagen V (Baghdadi et al., 2018). Future studies will be required to determine if TCDD exposure leads to modification of the MuSC niche or induces a cell autonomous mechanism to escape the quiescence signals from the local environment.

ACKNOWLEDGEMENTS

We warmly thank Aurélie Guguin, Adeline Henry and Magali Fradet for their assistance with flow cytometry. We also wish to thank Sonia Alonso-Martin for her technical support and scientific suggestions. We thank Nathalie Didier for assistance with the *Pax3*^{nlacZ-IRESGFP/+}

knock-in mouse line. We thank Camille Laisne, Diana Gelperowic, Christophe Boucly and Anna-Sophia Lourenco for animal care and animal facilities: Phénotypage du Petit Animal (NAC, UMS 028), Paris; Services des Animaux Transgéniques (SEAT, CNRS - UPS44), Villejuif for generating transgenic animals; CDTA (TAAM, CNRS – UPS44). Special thanks to Majorie Joiner, Stéphane Cardon and Sébastien Pelerin from ThermoFischer company for their expertise and the provision of the Attune® NxT Acoustic Focusing Flow Cytometer (Life Technologies). This work was supported by funding to FR from Association Française contre les Myopathies (AFM) via TRANSLAMUSCLE (PROJECT 19507), Labex REVIVE (ANR-10-LABX-73), Fondation pour la Recherche Médicale (FRM; Grant FDT20130928236 and DEQ20130326526), Agence Nationale pour la Recherche (ANR) grant Bone-muscle-repair (ANR-13-BSV1-0011-02), BMP-myomass (ANR-12-BSV1-0038-04), Satnet (ANR-15-CE13-0011-01), BMP-MyoStem (ANR-16-CE14-0002-03), MyoStemVasc (ANR-17-CE14-0018-01) and RHU CARMMA (ANR-15-RHUS-0003) and National Institutes of Health grant HL60714 to SJC.

AUTHOR CONTRIBUTIONS

Designed experiments, A.D.V., S.H., F.A. M.G. and F.R.; Performed experiments, A.D.V., M.G., M.Q., F.A., S.M., S.H., C.D., B.D.L., A.S.; Generated mouse models, F.A. D.R., S.J.C. and F.R.; Wrote the manuscript, A.D.V, M.G., S.M., F.A. and F.R.; Funding Acquisition, M.B., F.R., S.J.C.; Supervision, M.G. and F.R.

DECLARATION OF INTERESTS

The authors declare no competing interests.

MAIN FIGURE TITLES AND LEGENDS

Figure 1. Exposure to TCDD pollutant affects skeletal muscle homeostasis and MuSC number.

(A) Experimental design.

(B) Representative pictures of double immunofluorescence staining of LAMININ (purple) and embryonic Myosin Heavy Chain (eMHC, blue) on *Tibialis Anterior* (TA) or *Biceps brachii* (Biceps) muscle sections from mice treated with vehicle (nonane, top panel) or TCDD (4µg/kg, bottom panel). Scale bar, 40 µm.

(C) Quantification of eMHC positive myofibers performed on *Tibialis Anterior* (TA) or *Biceps brachii* (Biceps) muscle sections from mice treated with vehicle (nonane) or TCDD (4µg/kg). Means ± SEM (n=5), two-way ANOVA. *P* values calculated by Sidak's post-test. NS, not significant.

(D) Representative pictures of immunofluorescence staining of PAX7+ cells performed on *Extensor digitorum longus* (EDL), *Tibialis Anterior* (TA), *Biceps brachii* (Biceps) and diaphragm muscle sections from mice receiving vehicle (nonane) or TCDD (4µg/kg). Scale bar, 20 µm. BF, brightfield.

(E) Quantification of PAX7⁺ cells per surface area (mm²) performed on *Extensor digitorum longus* (EDL), *Tibialis Anterior* (TA), *Biceps brachii* (Biceps) and diaphragm muscle sections from mice receiving TCDD (4µg/kg) normalized to vehicle (nonane) condition in percentage. Means ± SEM (n=5), two-way ANOVA. *P* values calculated by Sidak's post-test. NS, not significant.

Figure 2. Differential loss of MuSCs exposed to TCDD is linked to muscle-specific expression of PAX3.

(A) Construction of *Pax3*^{nLacZ-IRESGFP/+} mice: a nls-LacZ IRES-GFP cassette was inserted into the translation start site in exon 1 of the *Pax3* gene to follow PAX3 spatiotemporal expression (see Material & methods for details).

(B) Representative picture of X-gal staining performed on different adult whole skeletal muscles from *Pax3*^{nLacZ-IRESGFP/+} adult (2 months) mice showing that PAX3-derived MuSCs subpopulation is differentially distributed within adult skeletal muscles. Scale bar, 1mm. TA: *Tibialis Anterior*, Gastro.: *Gastrocnemius* EDL: *Extensor Digitorum Longus*.

(C) Experimental design.

(D) Representative co-immunofluorescence staining of GFP (PAX3 reporter, green), PAX3 (red), and nuclei (DAPI, blue) performed on single myofibers. Scale bar 40µm. BF, brightfield.

(E) Representative co-immunofluorescence staining of GFP (PAX3 reporter, green), PAX3 (red), PAX7 (pink) and nuclei (DAPI, blue) performed on isolated MuSCs. Scale bar, 40µm (overview) or 5 µm (inset).

(F) Experimental design.

(G) Quantification of PAX7⁺ cells per surface area (mm²) performed on *Tibialis Anterior* (TA) and *Biceps brachii* (Biceps) muscle sections from mice receiving TCDD (4µg/kg) or vehicle (nonane) and analyzed at the end of 4 weeks-treatment period (10 weeks) or 2 months (18 weeks) post-treatment. Means ± SEM (n=4-6), two-way ANOVA. *P* values calculated by Sidak's post-test. NS, not significant.

Figure 3. Bimodal response of MuSCs to TCDD correlates with PAX3 expression

(A) Experimental design.

(B) Representative co-immunofluorescence staining of single myofibers from biceps isolated from mice receiving vehicle (nonane, top) or TCDD (4µg/kg, bottom), using antibodies against GFP (PAX3 reporter, green), PAX7 (pink), MYOD (red) and nuclei (DAPI, blue). White arrows indicate MuSCs and asterisks highlight PAX7⁻/MYOD⁺ MuSCs peculiar population. Scale bar, 40 µm.

(C) Quantification of **(B)** showing quiescent (PAX7⁺/MYOD⁻), activated (PAX7⁺/MYOD⁺) and differentiated (PAX7⁻/MYOD⁺) MuSCs within PAX3-negative (GFP⁻) and PAX3-positive (GFP⁺) MuSCs on single myofibers from biceps isolated from mice receiving vehicle (nonane) or TCDD (4µg/kg). Means ± SEM (n=4), two-way ANOVA. *P* values calculated by Sidak's post-test. NS, not significant.

(D) Experimental design.

(E) Representative co-immunofluorescence staining of single myofibers from biceps isolated from mice receiving vehicle (nonane, top) or TCDD (4µg/kg, bottom), using antibodies against GFP (PAX3 reporter, green), MYOG (red) and nuclei (DAPI, blue) at the end of the treatment (10 weeks), 1 month (14 weeks) or 2 months (18 weeks) post-treatment. White arrows indicate MYOG+ MuSC population. Scale bar, 10 µm.

(F) Quantification of **(E)** showing MYOG+ cells within PAX3-negative (GFP-) and PAX3-positive (GFP+) cells on single myofibers from biceps isolated from mice receiving vehicle (nonane) or TCDD (4µg/kg) at the end of the 4 week- treatment period (10 weeks), 1 month (14 weeks) or 2 months (18 weeks) post-treatment. Means ± SEM (n=4), two-way ANOVA. *P* values calculated by Sidak's post-test. NS, not significant.

(G) Experimental design.

(H) Quantification of living cells (Annexin V-; Sytox-), early apoptotic (Annexin V+; Sytox-), apoptotic (Annexin V+; Sytox+) and necrotic cells (Annexin V-; Sytox+) in PAX3- MuSCs (isolated from *Tg:Pax7nGFP* hindlimb muscles, left) or PAX3+ (isolated from *Pax3^{GFP/+}* trunk and forelimb muscles, right). Means ± SEM (n=4), Mann Whitney test. NS, not significant.

Figure 4. TCDD induces fusion of PAX3- MuSCs to myofibers without local injury.

(A) Schematic representation of *Tg:MyoD-nlacZ* reporter mice.

(B) Experimental design.

(C) Representative co-immunofluorescence staining of PAX7 (green), β-galactosidase (MYOD reporter, red) and nuclei (DAPI, blue) from TA or biceps upon vehicle (nonane) or TCDD (4µg/kg) treatment. Quiescent PAX7+/β-galactosidase- cells are shown with green arrows. PAX7+/β-galactosidase+ (activated or derived from activated) cells are shown with yellow arrows. Positive myofibers are labelled with an asterisk. Scale bar, 100µm.

(D-F) Quantifications of PAX7+/β-galactosidase- cells **(D)**, PAX7+/β-galactosidase+ cells **(E)** or β-galactosidase + myofibers derived from activated MYOD+ MuSCs **(F)** from TA or biceps upon vehicle (nonane) or TCDD (4µg/kg) treatment as shown in **(C)**. Means ± SEM (n=4), two-way ANOVA. *P* values calculated by Sidak's post-test. NS, not significant.

(G) Experimental design.

(H) Representative co-immunofluorescence staining of GFP (PAX3 reporter, green) and tomato (PAX7 reporter, red) on TA or biceps muscle cryosections after vehicle (nonane) or TCDD (4µg/kg) treatment. Positive myofibers for at least one channel are labelled with an asterisk. Scale bars, 600 µm (TA overview), 200 µm (Biceps overview), 30 µm (insets).

(I-J) Quantification of myofibers derived from PAX7+/PAX3- (GFP-) MuSCs (tomato labelled myofibers, red) and from PAX7+/PAX3+ (PAX3+) MuSCs (tomato and GFP labelled myofibers, red and green) from TA **(I)** or biceps **(J)** muscle cryosections after vehicle (nonane) or TCDD (4µg/kg) treatment as indicated and shown in **(H)**. Means ± SEM (n=4), two-way ANOVA. *P* values calculated by Sidak's post-test. NS, not significant.

(K) Experimental design.

(L) Quantification of the percentage of centronucleated fibers in *biceps brachii* (biceps) and *tibialis anterior* (TA) cryosections performed at the end of the 4 week-treatment period (10 weeks), 1 month (14 weeks) or 2 months (18 weeks) post-treatment. Means ± SEM (n=4-6) two-way ANOVA. *P* values calculated by Sidak's post-test. NS, not significant.

Figure 5. AHR signaling is required for MuSC activation in response to TCDD.

(A) Experimental design.

(B) Box plot showing the relative expression of AHR target genes (*Cyp1a1* and *AHRR*) and myogenic genes (*Pax3* and *MyoD*) normalized to *Tbp* and *Hprt1* in MuSCs isolated from AHR Ctrl (left panel) and AHR cKO (right panel) mice treated with vehicle (nonane) or TCDD (4µg/kg). Means ± SEM (n=4), two-way ANOVA. *P* values calculated by Sidak's post-test. NS, not significant.

(C) Representative co-immunofluorescence staining of *Tibialis anterior* (TA) isolated from AHR Ctrl and AHR cKO mice receiving vehicle (nonane, left) or TCDD (4µg/kg, right), using antibodies against, PAX7 (green), MYOD (red), KI67 (pink) and nuclei staining (DAPI, blue). Arrows show PAX7+ MuSCs. Scale bar, 40 µm. BF, brightfield.

(D) Quantification of quiescent (PAX7+/MYOD-/KI67-), activated (PAX7+/MYOD+/KI67-) and cycling (PAX7-/MYOD+/KI67+) MuSCs performed on TA muscle sections from the experiments shown in **(C)** in AHR Ctrl and AHR cKO mice treated with vehicle or TCDD (4µg/kg). Means ± SEM (n=4), two-way ANOVA. *P* values calculated by Sidak's post-test. NS, not significant.

Figure 6. Impairing PAX3 expression leads to MuSC sensitization to TCDD.

(A) Experimental design.

(B) MuSCs were isolated from Pax3 Ctrl or Pax3 cKO trunk and forelimb muscles by antibody-based flow cytometry combined with GFP reporter to distinguish PAX3+ (GFP+) from PAX3- (GFP-) MuSCs, from mice treated by vehicle (nonane) or TCDD (4µg/kg). Total RNA was extracted and gene expression study was performed by quantitative Polymerase Chain Reaction (qPCR). Relative expression to *Tbp* and *Hprt1* of target genes is shown in MuSCs from GFP- (PAX3-) or GFP+ (PAX3+) MuSCs. Means ± SEM (n=3), two-way ANOVA. *P* values calculated by Sidak's post-test. NS, not significant.

(C) Representative co-immunostaining of GFP (PAX3 reporter, green), PAX7 (pink) and MYOD (red) from biceps of Pax3 Ctrl and Pax3 cKO mice treated with vehicle or TCDD (4µg/kg). Scale bar, 20 µm.

(D) Quantification of quiescent (PAX7+/MYOD-) and activated (PAX7+/MYOD+) MuSCs from GFP- (PAX3-) or GFP+ (PAX3+) MuSCs in Pax3 Ctrl or Pax3 cKO mice, following treatment with vehicle (TCDD-) or TCDD (4µg/kg, TCDD+). Means ± SEM (n=3), two-way ANOVA. *P* values calculated by Sidak's post-test. NS, not significant.

(E) Experimental design.

(F) Representative co-immunofluorescence staining of AHR (red), GFP (PAX3 reporter, green), PAX7 (pink), and nuclei (DAPI, blue) from isolated biceps fibers of *Pax3*^{GFP/+} mice receiving vehicle (nonane) or TCDD (4µg/kg) as indicated. Scale bar, 10µm.

(G) Quantification of AHR localization observed in **(F)** within the PAX3-negative (GFP-) and PAX3-positive (GFP+) MuSCs. Means ± SEM (n=5), two-way ANOVA. *P* values calculated by Sidak's post-test. NS, not significant.

Figure 7. PAX3 expression controls the adaptive transition of quiescent MuSCs from G(0) to G(alert) through the mTORC1 pathway under environmental stress.

(A) Experimental design.

(B) EdU incorporation was quantified 12, 24 and 48h post-plating in GFP- and GFP+ MuSCs from mice treated with vehicle (nonane) or TCDD (4µg/kg). Means ± SEM (n=3), two-way ANOVA. *P* values calculated by Sidak's post-test. NS, not significant.

(C) Box and whiskers plots showing the diameter (µm) repartition of PAX3- (GFP-) or PAX3+ (GFP+) MuSCs from mice treated with vehicle (nonane) or TCDD (4µg/kg). Means (pink) ± SEM (n=4), two-way ANOVA. *P* values calculated by Sidak's post-test. NS, not significant.

(D) Quantification of mtDNA/genomic (g) DNA ratio by qRT-PCR in PAX3-negative (GFP-) and PAX3-positive (GFP+) MuSCs from mice treated with vehicle (nonane) or TCDD (4µg/kg). Means ± SEM (n=6), two-way ANOVA. *P* values calculated by Sidak's post-test. NS, not significant.

(E) Experimental design.

(F) Quantification of p-S6 immunofluorescence staining at the end of treatment (10 weeks) in Pax3 Ctrl or Pax3cKO mice and 1 month (14 weeks) or 2 months (18 weeks) post-treatment in *Pax3*^{GFP/+} mice. Means ± SEM (n=3-6), two-way ANOVA. *P* values calculated by Sidak's post-test. NS, not significant.

(G) Experimental design.

(H) Representative co-immunofluorescence staining of single myofibers from biceps isolated from TCDD-treated mice and incubated 15h with rapamycin or its vehicle (DMSO), using antibodies against GFP (PAX3 reporter, green), PAX7 (pink), p-S6 (red) and nuclear staining (DAPI, blue). Scale bar, 20 µm.

(I) Quantification of **(H)** showing p-S6+ cells on myofibers isolated from biceps of Pax3 Ctrl and Pax3 cKO mice receiving TCDD (4µg/kg) and incubated 15h with rapamycin or its vehicle. GFP- and GFP+ cells were quantified independently as indicated in either Pax3 ctrl or Pax3 cKO mice. Means ± SEM (n=3), two-way ANOVA. *P* values calculated by Sidak's post-test. NS, not significant.

(J) Representative co-immunofluorescence staining of single myofibers from biceps isolated from mice receiving TCDD (4µg/kg) and incubated 15h with rapamycin or its vehicle, using antibodies against GFP (PAX3 reporter, green), PAX7 (pink), MYOD (red) and nuclear staining (DAPI, blue). Scale bar, 20 µm.

(K) Quantification of **(J)** showing MYOD+ cells on myofibers isolated from biceps of Pax3 Ctrl and Pax3 cKO mice receiving TCDD (4µg/kg) treatment and incubated 15h with rapamycin or its vehicle. GFP- and GFP+ cells were quantified independently as indicated in either Pax3 ctrl or Pax3 cKO mice. Means ± SEM (n=3), two-way ANOVA. *P* values calculated by Sidak's post-test. NS, not significant.

MAIN TABLES AND LEGENDS

none

STAR METHODS

KEY RESOURCES TABLE

REAGENT or RESOURCE	SOURCE	IDENTIFIER
---------------------	--------	------------

Antibodies		
IgG rabbit polyclonal anti-AHR (H-211) (IF 1:200)	Santa Cruz	Cat# sc-5579 RRID:AB_633731
IgY chicken polyclonal anti-GFP (IF 1:500)	Abcam	Cat# ab13970 RRID:AB_300798
IgG rabbit polyclonal anti-Ki67 (SP6) (IF 1:200)	Abcam	Cat# ab16667 RRID:AB_302459
IgG rabbit polyclonal anti-Laminin (IF 1:1000)	Sigma-Aldrich	Cat# L9393 RRID:AB_477163
IgG2a rat monoclonal anti-MyoD (5F11) (IF 1:200)	Active Motif	Cat# 39991
IgG rabbit polyclonal anti-MyoD (M-318) (IF 1:200)	Santa Cruz	Cat# sc-760 RRID:AB_2148870
IgG1 mouse monoclonal anti-MyoG (F5D) (IF 1:200)	Invitrogen	Cat# MA5-11486 RRID:AB_10977211
IgG2a mouse monoclonal anti-Pax3 (Pax3-c) (IF 1:100)	DSHB	RRID:AB_528426
IgG1 mouse monoclonal anti-Pax7 (Pax7-c) (IF 1:100)	Santa Cruz	Cat# sc-81648 RRID:AB_2159836
IgG rabbit polyclonal anti-Pax7 (IF 1:100)	Aviva Systems Biology	Cat# ARP32742_P050 RRID : AB_387565
IgG1 mouse monoclonal anti-eMHC (IF 1:200)	Santa Cruz	Cat# sc-53091 RRID:AB_670121
IgG rabbit polyclonal anti-b-gal (IF 1:500)	Life Technologies	Cat# A-11132 RRID:AB_221539
IgG rabbit polyclonal anti-p-S6 (IF 1:200)	Cell Signaling	Cat# 2211 AB_331679
IgG goat polyclonal anti-Fab fragment (IF 1:1000)	Jackson ImmunoResearch	Cat# 115-007-003 RRID:AB_2338476
IgG2b rat polyclonal anti-Ter-119 PE-Cy7 (FACS 1:200)	BD Biosciences	Cat# 557853 RRID:AB_396898
IgG2b rat polyclonal anti-CD45 PE-Cy7 (FACS 1:200)	BD Biosciences	Cat# 552848 RRID:AB_394489
IgG2b rat polyclonal anti-Ly6A/E (Sca-1) PE (FACS 1:200)	BD Biosciences	Cat# 553108 RRID:AB_394629
IgG2a rat polyclonal anti-CD34 BV421 (FACS 1:100)	BD Biosciences	Cat# 552848 RRID:AB_394489
IgG2b rat polyclonal anti-a7 Integrin Alexa700 (FACS 1:70)	R&D Systems	Cat# FAB3518N RRID:AB_10973483
IgG rabbit polyclonal anti-AHR (H-211) (IF, WB 1:200)	Santa Cruz	Cat# sc-5579 RRID:AB_633731
IgG rabbit polyclonal anti-TBP (WB 1:1000)	Cell Signaling	Cat# 8515 RRID:AB_10949159
Chemicals, Peptides, and Recombinant Proteins		
Tamoxifen : 250 mk/kg diet	Genestil	Cat#1324P
2,3,7,8-Tetrachlorodibenzo-p-dioxin 50 µg/mL in Nonane	LGC standards	Cat#CIL-ED-901
n-Nonane Picograde® for residue analysis	LGC standards	Cat#SO-1271-B010
Corn oil	Sigma	Cat#C8267
Dispase® II (neutral protease, grade II)	Roche	Cat#04942078001
Collagenase A	Roche	Cat#11088793001
Pacific Blue™ Annexin V/SYTOX™ AADvanced™ Apoptosis Kit, for flow cytometry	Invitrogen™	Cat#A35136
Vybrant® DyeCycle™ Ruby cell permeable stain	Invitrogen™	Cat#V10273
Target Retrieval Solution, Citrate pH 6.1 (10x)	Dako	Cat#S2369
X-Gal	Sigma-Aldrich	Cat#7240-90-6

Chicken embryo extract	MP-Biomedical	Cat#CE-650-J
Rapamycin	Sigma-Aldrich	Cat#R8781
Fluoromount-G™ medium	Interchim	Cat#FP-483331
Collagenase type I	Sigma-Aldrich	Cat#C0130
ECL™ Blotting Reagents	Amersham Biosciences	Cat#GERPN2109
RNAqueous™-Micro Total RNA Isolation Kit™	Invitrogen™	Cat#AM1931
SuperScript™ VILOTM cDNA Synthesis Kit	Invitrogen™	Cat#11755-050
SuperScript™ IV VILO™ Master Mix with ezDNase™ Enzyme	Invitrogen™	Cat#11766050
SYBR™ Green Master Mix	Applied Biosystems™	Cat#4309155
TaqMan™ Gene Expression Master Mix	Applied Biosystems™	Cat#4369016
Click-iT™ Plus EdU Alexa Fluor™ 647 Imaging Kit	Invitrogen™	Cat#C10640
QIamp DNA micro kit	Qiagen	Cat#56304
Cytochrome B region on mtDNA (TaqMan, Mouse)	Applied Biosystems™	Mm04225271_g1 CYTB
β-globin region on gDNA (Taqman, Mouse)	Applied Biosystems™	Mm 01611268_g1 Hbb-b1
Critical Commercial Assays		
Phusion® High-Fidelity DNA Polymerase	Thermo Fisher Scientific™	Cat#F530L
pGEM®-T Easy Vector Systems	Promega	Cat#A3610
NucleoBond® BAC 100	Macherey-Nagel	Cat#740579
Experimental Models: Organisms/Strains		
C57BL/6N mice	Janvier Labs®	N/A
<i>Pax3^{GFP/+}</i> mice	Relaix et al., 2005	N/A
<i>Pax3^{flox/+}</i> mice	Koushik et al., 2002	N/A
Rosa26 ^{flox(stop)flox} -Tomato mice (R26 ^{stop} -Tomato)	Madisen et al., 2010	N/A
<i>Pax7^{creERT2/+}</i> mice	Murphy et al., 2011	N/A
Tg:Pax7-nGFP mice	Sambasivan et al., 2009	N/A
<i>AHR^{flox/flox}</i> mice	Walisser et al., 2005	N/A
Tg:MyoD-nLacZ mice	In this article	N/A
<i>Pax3^{nLacZ-IRESGFP/+}</i> mice	In this article	N/A
Oligonucleotides		
MyoD locus 5' homologous arm pair forward 5'-ATGATTCCCCTACGCATGCAAGGACAGCGC-3',	In this article	N/A
MyoD locus 5' homologous arm pair reverse 5'-ACTCGAGTTCCTGGGTCCAGCCTCAACCCAAGCCG-3'	In this article	N/A
MyoD locus 3' homologous arm pair forward 5'-ACTCGAGCACTACAGTGGCGACTCAGATGC-3',	In this article	N/A
MyoD locus 3' homologous arm pair reverse 5'-ATAACAGAGTTAGGTCTACAGGGCC-3'	In this article	N/A
Primers for Real-time qPCR, see Table S1	In this article	N/A
Recombinant DNA		
BAC clone	CHORI BACPAC resources	RP23-46A24
Software and Algorithms		

GraphPad Prism version 7.00 for MAC	La Jolla California USA, www.graphpad.com	N/A
Fiji software	Schindelin, J.; Arganda-Carreras, I. & Frise, E. et al. (2012)	N/A
Amnis® ImageStream® cell analysis	Amnis®	N/A
Zen Blue 2.0 software	Zeiss	N/A
ImageJ (version 1.47 v)	National Institutes of Health, USA, https://imagej.nih.gov.gate2.inist.fr/ij/	N/A
Other		
DS-11 FX spectrometer	DeNovix	N/A
Veriti® 96- Well Fast Thermal Cycler	Applied Biosystems™	N/A
StepOnePlus real-time PCR system	Applied Biosystems™	N/A
Attune® NxT Acoustic Focusing Flow Cytometer	Thermo Fisher Scientific™	N/A
LSM800 confocal	Zeiss	N/A
CCD camera Olympus model mounted on an binocular loupe	Leica	N/A
Axiolmager D1, fluorescence microscope	Zeiss	N/A

CONTACT FOR REAGENT AND RESOURCE SHARING

Further information and requests for resources and reagents should be directed to and will be fulfilled by the Lead Contact, Frédéric Relaix (frederic.relaix@inserm.fr).

EXPERIMENTAL MODEL AND SUBJECT DETAILS

Mouse strains

Mouse lines used in this study have been described and provided by the corresponding laboratories: C57BL/6N mice (Janvier Labs®), *Pax3*^{GFP/+} mice (Relaix et al., 2005), *Pax3*^{flox/+} (Koushik et al., 2002), *Rosa26*^{flox(stop)/flox-Tomato} (*R26*^{stop-Tomato}) (Madisen et al., 2010), *Pax7*^{creERT2/+} mice (Murphy et al., 2011), *Tg:Pax7-nGFP* (Sambasivan et al., 2009) and *AHR*^{flox/flox} mice (Walisser et al., 2005). *Tg:MyoD-nLacZ*, and *Pax3*^{nLacZ-IRESGFP/+} mice were generated in the laboratory (see below). Animals were handled according to national and European community guidelines, and protocols were approved by the ethics committee at the French Ministry (Project No: 15-018).

Generation of *Pax3*^{nLacZ-IRES-GFP/+} mice

The *Pax3* targeting construct is derived from one which was previously reported (Relaix et al., 2003). Briefly, a cassette containing a floxed *Pax3* cDNA followed with an nls-LacZ-IRES-eGFP-SV40pA replaces the coding sequence of exon1. The *Pax3*^{Pax3(nLacZ-IRES-eGFP)} targeting vector was electroporated in CK35 ES cells. Recombinant ES cells were analysed, and two

positive ES clones were injected into blastocysts to generate chimaeras. Following germline transmission and validation of the expression profile and appropriate recombination, the *Pax3*^{*Pax3*^{*nLacZ-IRESeGFP*}} allele has been established and will be reported elsewhere. A male carrying the recombined allele was later crossed with a PGK-Cre female (Lallemand et al., 1998) to flox out the *Pax3* cDNA and gave rise to the *Pax3*^{*nLacZ-IRESeGFP/+*} line.

Generation of *Tg:MyoD-nLacZ* mice

To generate a *Tg:MyoD-nLacZ* transgenic reporter line, a 227kb BAC clone from a C57BL/6J mice genomic library (Osoegawa et al., 2000) centered around the MyoD locus has been chosen (RP23-46A24 ; CHORI BACPAC resources) to carry out locus modifications using λ -red recombination (Copeland et al., 2001). Two homology arms were designed to target the start of the MyoD coding sequence in exon1, resulting in the deletion of 566bp of 5' CDS and replacement with the nls-lacZ sequence. DNA fragments were PCR-generated using the BAC DNA as template (PHUSION enzyme F-530L, Thermofischer) (5'arm pair 5'-ATGATTCCCCTACGCATGCAAGGACAGCGC-3', 5'-ACTCGAGTTCCTGGGTCCAGCCTCAACCCAAGCCG-3'; 3'arm pair 5'-ACTCGAGCACTACAGTGGCGACTCAGATGC-3', 5'-ATAACAGAGTTAGGTCTACAGGGCC-3'), then subcloned in pGEMTeasy (Promega #A3610) with a newly introduced XhoI site in-between. A nls-LacZ-SV40pA-FRT-Kanamycin-FRT cassette was then inserted in XhoI to give the final targeting construct. The 5.7kb targeting fragment was obtained by NotI digestion followed by gel purification. The BAC RP23-46A24 DNA was purified (Nucleobond BAC100, Macherey-Nagel) and electroporated into recombineering strain SW105 (Lee et al., 2001), several transformants DNA were extracted and verified by restriction profile against the parental DNA. The purified recombination cassette was then electroporated in one verified clone, and recombinant resulting clones, selected on Kanamycin, were analyzed by restriction profile for proper cassette integration. One positive clone was then grown on arabinose to induce Flp recombinase expression and promote excision of the selection marker. Recombined BAC DNA was purified and diluted at 2ng/ μ l into microinjection buffer (10mM Tris-HCL pH 7.0, 1mM EDTA, 100mM NaCl, +30mM Spermine and 70 mM Spermidine, extemporaneously) and injected into C57Bl/6xDBA/2 pronuclei. Positive F0 clones were selected by PCR and X-Gal profile of F1 offspring.

METHOD DETAILS

Tamoxifen and TCDD treatment

To induce recombination, four week-old *Pax3*^{*GFP/+*}; *Pax7*^{*CreERT2/+*}; *R26*^{*stop-Tomato*} or *Pax7*^{*CreERT2/+*}; *Pax3*^{*GFP/flox*} or *Pax7*^{*CreERT2/+*}; *AHR*^{*flox/flox*} mice were fed with a diet containing tamoxifen (Envigo) for ten consecutive days followed by 5 days of normal diet before TCDD treatment. Mice fed with normal diet were used as control. For TCDD treatment, six week-old *Tg:MyoD-nLacZ* or *Pax3*^{*nLacZ-IRESeGFP/+*} or *Pax3*^{*GFP/+*}; *Pax7*^{*CreERT2/+*}; *R26*^{*stop-Tomato*} or *Pax7*^{*CreERT2/+*}; *Pax3*^{*GFP/flox*} or *Pax7*^{*CreERT2/+*}; *AHR*^{*flox/flox*} mutant mice and their corresponding controls without tamoxifen were intraperitoneally injected with TCDD (4 μ g/kg) (LGC standards), every 2 or 3 days, 2

times per week for four weeks. Control mice (vehicle) were injected at the same frequency with the equivalent volume of Nonane or (TCDD diluent) in corn oil.

Muscle enzymatic dissociation

Adult forelimb, trunk or hindlimb muscles were dissected, minced and incubated with a mix of 2.4 U/ml Dispase II (Roche) and 100 µg/ml collagenase A (Roche) in cold 4.5g/L glucose Dulbecco's modified Eagle's medium (DMEM, Gibco) at 37 °C for 2 h. The muscle suspension was successively filtered through 100-µm and 70-µm cell strainers (BD Biosciences) and then spun at 50g for 10 min at 4 °C to remove large tissue fragments. The supernatant was collected, filtered through a 40 µm strainer and washed twice by centrifugation at 600g for 15 min at 4 °C. The final pellet was resuspended in cold 4.5g/L glucose DMEM) supplemented with 0.2% bovine serum albumin (BSA, Sigma), and the cell suspension was used for fluorescence-activated cell sorting (FACS)-sorting, the Amnis® ImageStream® cell analysis system or the apoptosis analysis.

MuSC isolation by Flow Cytometry

MuSCs were sorted from dissociated muscles with the cell sorter BD Influx Sorp (BD Biosciences) using either the GFP (for *Tg:Pax7-nGFP* or *Pax3^{GFP/+}* or *Pax3^{GFP/flox}* mice models) reporter or a surface labeling strategy (for *Pax7^{creERT2/+}*; *AHR^{flox/flox}* and *Pax7^{creERT2/+}*; *Pax3^{GFP/flox}* mice models) using anti-mouse CD45-PE-Cy7, anti-Ter119-PE-Cy7, anti-mouse CD34-BV421, anti-mouse Sca1-FITC (all from BD Biosciences) and anti-mouse integrin-α7-A700 (R&D Systems) (Stantzou et al., 2017). Gating strategy for satellite cell isolation using cell surface markers was as followed: Ter119⁻, CD45⁻, CD34⁺, Sca1⁻ and gating on the cell fraction integrin-α7⁺. In the *Pax7^{creERT2/+}*; *Pax3^{GFP/flox}* mice the PAX3⁺ MuSCs were isolated based on GFP from the Ter119⁻, CD45⁻, CD34⁺, Sca1⁻ and integrin-α7⁺ MuSCs fraction. Isolated, mononuclear cells were collected in DMEM/0.2% BSA. Sorted cells were either plated or lysed for mRNA extraction following the protocols described below.

Apoptosis assay by flow cytometry

Enzymatic dissociated muscles from *Tg:Pax7-nGFP* or *Pax3^{GFP/+}* mice were labeled with Pacific Blue™ Annexin V and SYTOX™ AADvanced™ dyes, according to manufacturer's recommendations (Pacific Blue™ Annexin V/SYTOX™ AADvanced™ Apoptosis Kit, for flow cytometry, Invitrogen™). Flow cytometry was performed using The Attune® NxT Acoustic Focusing Flow Cytometer (Life Technologies). Analysis was focused on the GFP⁺ cell subpopulation. Gates were drawn on bivariate SYTOX/Annexin V dot plots around four distinct subpopulations: SYTOX⁺/Annexin V⁻ (dead cells), SYTOX⁻/Annexin V⁺ (early apoptotic cells), SYTOX⁺/Annexin V⁺ (late apoptotic cells) and SYTOX⁻/Annexin V⁻ (living cells).

ImageStream®^x system analysis of cell size

Satellite cells isolated by FACS from *Tg:Pax7-nGFP* or *Pax3^{GFP/+}* mice were resuspended in 1 x PBS and stained with Vybrant® DyeCycle™ Ruby cell permeable stain (Invitrogen™) for 15 min at 37°C to identify the nucleus and ensure that MuSCs were not activated by the procedure. Samples were run directly on the Amnis® ImageStream®X cytometer equipped with a hydrodynamic focusing (Amnis part of EMD Millipore, Proteigene). For each condition (vehicle and TCDD-treated PAX3+ and PAX3- MuSCs) 5000 images were acquired using the brightfield laser (for the size of MuSCs), the darkfield laser (for the Side Scatter) and the fluorescence laser (for Vybrant® DyeCycle™ Ruby and GFP). The acquired images were analyzed with IDEAS software (Amnis). First, a scatter plot of aspect ratio/area was used to gate for single cells. Second, a gradient RMS (root mean square for image sharpness) histogram was used to gate for cells in focus. Third, the intensities of GFP and Vybrant® DyeCycle™ Ruby staining were used to ensure the non-activation of MuSCs. On the remaining living, single cells in focus, image analysis was performed to determine the size of the MuSCs by generating a mask based on brightfield. This methodology was used to compare the size of PAX3- and PAX3+ MuSCs.

Satellite cell culture

Satellite cells isolated by flow cytometry were plated at 25 000 cells per cm² on detachable 8 well-PCA treated μ -slides (Sarstedt) pre-coated with 0.2% gelatin for 30 min at 37 °C. Cells were cultured in satellite cell growth medium containing DMEM High glucose (Gibco) supplemented 20% FBS (Gibco) and primocin (100 μ g/ml, Invitrogen™) at 37 °C, 5% CO₂ for 2h before being fixed with 4% PFA and immunostained as described in “Immunostaining on cells, sections and myofibers”.

Muscle fixation, histological analysis and X-gal staining

For immunostaining experiments, adult *tibialis anterior* (TA), diaphragm, *extensor digitorum longus* (EDL) or *biceps brachii* (biceps) muscles were isolated and immediately frozen in liquid-nitrogen-cooled isopentane and sectioned transversely at 8 μ m. Muscle sections were post-fixed with 4% PFA, 20 min at room temperature, washed with 1x PBS (3 times) and permeabilized for 6 minutes with cold methanol (-20°C). After 3 washes with 1x PBS, antigen retrieval was performed by incubating sections in boiling 10 mM citrate buffer pH 6 (Dako) for 3 min. After cooling down 30min at room temperature, sections were washed 3 times with 1x PBS. Sections were then blocked with 2.5% BSA (Sigma) in PBS. BSA was removed and sections were incubated 30 min with Fab antibody. After 3 washes of 1x PBS, sections were incubated with primary and secondary antibodies as described in “Immunostaining on cells, sections and myofibers”.

For X-gal staining, isolated whole muscles from two-month *Pax3n^{LacZ-IRES-GFP/+}* mice were fixed on ice with 4% PFA for 2 h. After 3 washes with 1x PBS, the muscles were incubated in the X-Gal staining solution, using 0.4 mg/ml X-Gal (Sigma) in 2 mM MgCl₂, 0.02% NP-40, 0.1 M phosphate buffer (pH 7.4), 20 mM K₄Fe(CN)₆ and 20 mM K₃Fe(CN)₆ at 37°C for 16 h. Images were captured with a CCD camera Olympus model mounted on an binocular loupe (Leica).

Single myofiber isolation and rapamycin treatment

Single myofibers were isolated from EDL or biceps muscles following the previously

described protocol (Moyle and Zammit, 2014). Briefly, both muscles were dissected and digested in a filtered solution of 0.2% collagenase (Sigma) in DMEM High Glucose /1% L-Glutamine/1% Penicillin/Streptomycin (Gibco®) for 1h30 at 37°C. After connective tissue digestion, mechanical dissociation was performed to release individual myofibers that were then transferred to serum-coated Petri dishes for 20 min. Single myofibers were then immediately fixed in 4% PFA for 10 min (T0h). After 3 washes with 1x PBS, myofibers were stored at 4°C before immunostaining. In some experiments, freshly isolated myofibers were treated with 100 nM rapamycin (Sigma) for 15h in myofiber growth medium containing DMEM High glucose (Gibco®), 20% FBS (Gibco®) and 1% chicken embryo extract (MP-Biomedical) at 37°C, 5% CO₂ and then recovered for fixation and immunostaining as described in “Immunostaining on cells, sections and myofibers”.

Immunostaining on cells, sections and myofibers

Isolated MuSCs, muscles section or myofibers were washed three times with 1x PBS, and incubated overnight at 4°C in 2.5% BSA in 0.025% PBS-Tween20 with primary antibodies listed in **Key Resources Table**. Samples were washed 3 times with 0.025% PBS-Tween20 and incubated with Alexa-conjugated secondary antibodies (Life Technologies, 1/1000^e) for 1 h. After washing 3 times with 1X PBS, DAPI (Sigma, 1/5000^e) was added for 5 min at room temperature. Samples were washed 3 times with 1X PBS and slides were mounted with Fluoromount-G™ medium (Interchim). Confocal images were acquired with a Zeiss LSM800 confocal (Zeiss) for representative pictures and analyzed with Zen Blue 2.0 software. Counting was performed using ImageJ (version 1.47 v; National Institutes of Health, USA, <https://imagej.nih.gov/gate2.inist.fr/ij/>) or under the Zeiss fluorescence microscope (AxioImager D1, Zeiss).

Protein extraction and immunoblots

Satellite cells were isolated by FACS from *Pax7^{CreERT2/+}; AHR^{fl/fl}* mice that were fed with tamoxifen-diet (AHR cKO) or regular diet (AHR Ctrl) for 10 days. Cell lysates were prepared with ice-cold 0.5% deoxycholate, 0.1% SDS and 1% triton in 50 mM Tris-HCl, pH7.4, 150 mM NaCl, 1 mM EDTA, 1 mM Na₃VO₄, and protease inhibitor cocktail (1/100^e, Sigma). Lysates were then subjected to SDS-PAGE and transferred to polyvinylidene difluoride (PVDF) membranes. The membranes were probed overnight with anti-AHR or anti-TBP primary antibody at 4°C (see **Key Resources Table**). Signal was detected using ECL system (Amersham Biosciences) according to the manufacturer’s instructions. Quantitative analysis was performed using ImageJ software.

RNA isolation and RT-qPCR

Total RNA was extracted from satellite cells isolated by FACS using RNAqueous™-Micro Total RNA Isolation Kit™ (Invitrogen™) and cDNA synthesis was performed using SuperScript™ VILO™ cDNA Synthesis Kit (Invitrogen™) or SuperScript™ IV VILO™ Master Mix with ezDNase™ Enzyme respectively for the experiments in *Pax7^{CreERT2/+}; AHR^{flox/flox}* and *Pax7^{CreERT2/+}; Pax3^{GFP/flox}* mice models according to manufacturer’s instructions. RNA quality was assessed by spectrophotometry (DeNovix DS-11 FX spectrometer). RT-PCR was performed using the Veriti® 96- Well Fast Thermal Cycler (Applied Biosystems™) and real-time qPCR was performed with the StepOnePlus real-time PCR system (Applied

Biosystems™) using SYBR™ Green detection tools (Applied Biosystems™). Expression of each gene was normalized to TATA Box Protein (*Tbp*) and Hypoxanthine Phosphoribosyltransferase 1 (*Hprt1*) genes expression. Results are reported as relative gene expression ($2^{-\Delta\Delta CT}$) using vehicle treated-control mice as reference (Livak and Schmittgen, 2001). Specific forward and reverse primers used in this study are listed in **Table S1**.

Cell cycle kinetics

An EdU pulse (for 4h) at a final concentration of 10 μ M was added to 25 000 MuSCs isolated and plated in 8 well chamber slide pre-coated with 0.2 % of PBS-gelatin. EdU incorporation was analyzed 12, 24 and 48 hours after cells plating using the Click-iT™ Plus EdU Alexa Fluor™ 647 Imaging Kit (Invitrogen™).

mtDNA quantification

Total DNA was isolated from 25 000 MuSCs immediately after FACS isolation using QIAmp DNA micro kit (Qiagen) according to the manufacturer's instructions. Mitochondrial (mt) DNA was quantified by qRT-PCR using primers amplifying the Cytochrome B region on mtDNA (TaqMan, Mouse: Mm04225271_g1 CYTB) relative to the β -globin region on gDNA (Taqman, Mouse: Mm 01611268_g1 Hbb-b1).

QUANTIFICATION AND STATISTICAL ANALYSIS

Statistical analysis

Experiments involving mice were performed with a minimum of three to six biological replicates (as indicated in each legend of the figure) and results are presented as the mean \pm S.E.M. For technical replications, six to nine cryosections were analyzed per muscle and per mice, a minimum of fifty to eighty fibers were taken for single myofibers analysis. For qPCR analysis 100 000 cells were used per conditions and per mice. All statistical analysis and graphs were performed using GraphPad Prism® Software (version 7.0). Statistical two-way ANOVA tests are detailed for each figure as below:

Figure 1C: Means \pm SEM (n=5), Repeated measure (RM) two-way ANOVA. Repeated measures: muscles per conditions. Source of variation: variable 1, treatment: $p < 0.0001$; variable 2, type of muscle: $p = 0.0343$; interaction $p = 0.0035$. ANOVA was followed by Sidak's post-test. P values between the groups (Vehicle vs. TCDD or TA vs. Biceps) in Sidak's post-test are shown at the top of the panel (NS, not significant).

Figure 1E: Means \pm SEM (n=6), RM two-way ANOVA. Repeated measure: muscles per conditions. Source of variation: variable 1, treatment: $p < 0.0001$; variable 2, type of muscle: $p < 0.0001$; interaction $p < 0.0001$. ANOVA was followed by Sidak's post-test. P values between the groups (Vehicle vs. TCDD or between muscles) in Sidak's post-test are shown at the top of the panel (NS, not significant).

Figure 2G: Means \pm SEM (n=6 for 10 weeks and n=4 for 18 weeks), RM two-way ANOVA. Repeated measure: PAX3- and PAX3+ MuSCs per conditions. Source of variation: variable 1, treatment: p<0.0001 (10 weeks) p=0.0050 (18 weeks); variable 2, MuSCs subpopulation: p=0.0025 (10 weeks), p=0.0157 (18 weeks); interaction p<0.0001 (for both 10 and 18 weeks). ANOVA was followed by Sidak's post-test. P values between the groups (Vehicle vs. TCDD) in Sidak's post-test are shown at the top of the panel (NS, not significant).

Figure 3C: Means \pm SEM (n=4), RM two-way ANOVA. Repeated measure: PAX3- and PAX3+ MuSCs per conditions. Source of variation: variable 1, treatment: p=0.0008 (quiescent), p=0.0016 (activated), p=0.0011 (differentiated); variable 2, MuSCs subpopulation: p=0.0079 (quiescent), p=0.0235 (activated), p=0.0011 (differentiated); interaction: p=0.0134 (quiescent), p=0.0370 (activated), p=0.0011 (differentiated). ANOVA was followed by Sidak's post-test. P values between the groups (Vehicle vs. TCDD or between PAX3- and PAX3+ MuSC subpopulations) in Sidak's post-test are shown at the top of the panel (NS, not significant).

Figure 3F: Means \pm SEM (n=5 for 10 weeks, n=4 for both 14 and 18 weeks), RM two-way ANOVA. Repeated measure: PAX3- and PAX3+ MuSCs per conditions. Source of variation: variable 1, treatment: p<0.0001 (10 weeks), p=0.0011 (14 weeks), p=0.0016 (18 weeks); variable 2, MuSC subpopulations: p<0.0001 (10 weeks), p=0.0011 (14 weeks), p=0.0100 (18 weeks); interaction: p<0.0001 (10 weeks), p=0.0011 (14 weeks), p=0.0016 (18 weeks). ANOVA was followed by Sidak's post-test. P values between the groups (Vehicle vs. TCDD or between PAX3- and PAX3+ MuSC subpopulations) in Sidak's post-test are shown at the top of the panel (NS, not significant).

Figure 4D: Means \pm SEM (n=4), RM two-way ANOVA. Repeated measure: muscles per conditions. Source of variation: variable 1, treatment: p<0.0001; variable 2, Muscle: p=0.0256; interaction: p=0.0161. ANOVA was followed by Sidak's post-test. P values between the groups (Vehicle vs. TCDD or between muscles) in Sidak's post-test are shown at the top of the panel (NS, not significant).

Figure 4E: Means \pm SEM (n=4), RM two-way ANOVA. Repeated measure: muscles per conditions. Source of variation: variable 1, treatment: p<0.0001; variable 2, Muscle: p=0.0256; interaction: p=0.0161. ANOVA was followed by Sidak's post-test. P values between the groups (Vehicle vs. TCDD or between muscles) in Sidak's post-test are shown at the top of the panel (NS, not significant).

Figure 4F: Means \pm SEM (n=4), RM two-way ANOVA. Repeated measure: muscles per conditions. Source of variation: variable 1, treatment: p=0.0002; variable 2, Muscle: p=0.0301; interaction: p=0.0124. ANOVA was followed by Sidak's post-test. P values between the groups (Vehicle vs. TCDD or between muscles) in Sidak's post-test are shown at the top of the panel (NS, not significant).

Figure 4I: Means \pm SEM (n=4), RM two-way ANOVA. Repeated measure: MuSCs subpopulation per conditions. Source of variation: variable 1, treatment: p=0.0021; variable 2, MuSCs subpopulation: p=0.0004; interaction: p=0.0021. ANOVA was followed by Sidak's post-test. P values between the groups (Vehicle vs. TCDD or between PAX3- and PAX3+

MuSC subpopulations) in Sidak's post-test are shown at the top of the panel (NS, not significant).

Figure 4J: Means \pm SEM (n=4), RM two-way ANOVA. Repeated measure: MuSCs subpopulation per conditions. Source of variation: variable 1, treatment: p=0.0247; variable 2, MuSCs subpopulation: p=0.0018; interaction: p=0.0368. ANOVA was followed by Sidak's post-test. P values between the groups (Vehicle vs. TCDD or between PAX3- and PAX3+ MuSC subpopulations) in Sidak's post-test are shown at the top of the panel (NS, not significant).

Figure 4L: Means \pm SEM (n=6 for 10 weeks and n=4 for 14 and 18 weeks), RM two-way ANOVA. Repeated measure: muscle per condition. Source of variation: variable 1, treatment: p<0.0001 (10 weeks), p=0.0009 (14 weeks), p=0.0005 (18 weeks); variable 2, muscle: p=0.0244 (10 weeks), p=0.0016 (14 weeks), p=0.1564 (18 weeks); interaction: p=0.0878 (10 weeks), p=0.0024 (14 weeks), p=0.0411 (18 weeks). ANOVA was followed by Sidak's post-test. P values between the groups (Vehicle vs. TCDD or between muscles) in Sidak's post-test are shown at the top of the panel (NS, not significant).

Figures 5B and S3D: Means \pm SEM (n=4), ordinary two-way ANOVA, groups: AHR Ctrl vehicle vs AHR Ctrl TCDD vs AHR cKO vehicle vs AHR cKO TCDD. ANOVAs results are detailed below:

- *Cyp1a1*: Source of variation: variable 1, treatment: p<0.0001; variable 2, genotype: p=0.0033; interaction: p=0.0047.
- *AHRR*: Source of variation: variable 1, treatment: p<0.0001; variable 2, genotype: p<0.0001; interaction: p<0.0001.
- *Pax3*: Source of variation: variable 1, treatment: p=0.0006; variable 2, genotype: p=0.0358; interaction: p=0.0304.
- *MyoD*: Source of variation: variable 1, treatment: p=0.0138; variable 2, genotype: p=0.1065; interaction: p=0.0288.
- *Nqo1*: Source of variation: variable 1, treatment: p=0.0002; variable 2, genotype: p=0.0757; interaction: p=0.5932.
- *Cyp1a2*: Source of variation: variable 1, treatment: p<0.0001; variable 2, genotype: p=0.0003; interaction: p=0.0001.
- *Cyp1b1*: Source of variation: variable 1, treatment: p=0.0319; variable 2, genotype: p=0.1474; interaction: p=0.0496.

ANOVA was followed by Sidak's post-test. P values between the groups (Vehicle vs. TCDD or between Ctrl vs. cKO) in Sidak's post-test are shown at the top of the panel (NS, not significant).

Figure 5D: Means \pm SEM (n=4), ordinary two-way ANOVA, groups: AHR Ctrl vehicle vs AHR Ctrl TCDD vs AHR cKO vehicle vs AHR cKO TCDD. ANOVAs results are detailed below:

- *PAX7+/MYOD-/Ki67-*: Source of variation: variable 1, treatment: $p < 0.0001$; variable 2, genotype: $p = 0.0006$; interaction: $p = 0.0020$.
- *PAX7+/MYOD+/Ki67-*: Source of variation: variable 1, treatment: $p < 0.0001$; variable 2, genotype: $p = 0.0025$; interaction: $p = 0.0051$.
- *PAX7+/MYOD+/Ki67+*: Source of variation: variable 1, treatment: $p < 0.0001$; variable 2, genotype: $p = 0.0041$; interaction: $p = 0.0272$.

ANOVAs were followed by Sidak's post-test. *P* values between the groups (Vehicle vs. TCDD or between Ctrl vs. cKO) in Sidak's post-test are shown at the top of the panel (NS, not significant).

Figure S3G: Means \pm SEM ($n=4$), ordinary two-way ANOVA, groups: AHR Ctrl vehicle vs AHR Ctrl TCDD vs AHR cKO vehicle vs AHR cKO TCDD. ANOVAs results are detailed below:

- *PAX7+/MYOD-/Ki67-*: Source of variation: variable 1, treatment: $p < 0.0001$; variable 2, genotype: $p < 0.0001$; interaction: $p < 0.0001$.
- *PAX7+/MYOD+/Ki67-*: Source of variation: variable 1, treatment: $p < 0.0001$; variable 2, genotype: $p < 0.0001$; interaction: $p = 0.0002$.
- *PAX7+/MYOD+/Ki67+*: Source of variation: variable 1, treatment: $p = 0.0003$; variable 2, genotype: $p = 0.0003$; interaction: $p = 0.0003$.

ANOVAs were followed by Sidak's post-test. *P* values between the groups (Vehicle vs. TCDD or between Ctrl vs. cKO) in Sidak's post-test are shown at the top of the panel (NS, not significant).

Figures 6B and S4B: Means \pm SEM ($n=3$), repeated measure (RM) two-way ANOVA, groups: GFP- vehicle vs GFP- TCDD vs GFP+ vehicle vs GFP+ TCDD. ANOVAs were performed in each mice genotype (Pax3 Ctrl or Pax3 cKO). Repeated measure: PAX3- and PAX3+ MuSC subpopulations per conditions. ANOVAs results are detailed below:

- Pax3 Ctrl, *Pax3*: Source of variation: variable 1, treatment: $p = 0.3888$; variable 2, PAX3- and PAX3+ MuSC subpopulations: $p = 0.0021$; interaction: $p = 0.2372$.
- Pax3 cKO, *Pax3*: Source of variation: variable 1, treatment: $p = 0.4859$; variable 2, PAX3- and PAX3+ MuSC subpopulations: $p = 0.5565$; interaction: $p = 0.6981$.
- Pax3 Ctrl, *Cyp1a1*: Source of variation: variable 1, treatment: $p = 0.0032$; variable 2, PAX3- and PAX3+ MuSC subpopulations: $p = 0.0348$; interaction: $p = 0.0451$.
- Pax3 cKO, *Cyp1a1*: Source of variation: variable 1, treatment: $p = 0.0052$; variable 2, PAX3- and PAX3+ MuSC subpopulations: $p = 0.7648$; interaction: $p = 0.7217$.
- Pax3 Ctrl, *MyoD*: Source of variation: variable 1, treatment: $p = 0.1127$; variable 2, PAX3- and PAX3+ MuSC subpopulations: $p = 0.0372$; interaction: $p = 0.0350$.
- Pax3 cKO, *MyoD*: Source of variation: variable 1, treatment: $p = 0.0048$; variable 2, PAX3- and PAX3+ MuSC subpopulations: $p = 0.0264$; interaction: $p = 0.5127$.

- Pax3 Ctrl, *AHRR*: Source of variation: variable 1, treatment: p=0.0079; variable 2, PAX3- and PAX3+ MuSC subpopulations: p=0.0065; interaction: p=0.0065.
- Pax3 cKO, *AHRR*: Source of variation: variable 1, treatment: p=0.0084; variable 2, PAX3- and PAX3+ MuSC subpopulations: p=0.5147; interaction: p=0.3245.
- Pax3 Ctrl, *Nqo1*: Source of variation: variable 1, treatment: p=0.0003; variable 2, PAX3- and PAX3+ MuSC subpopulations: p=0.2348; interaction: p=0.0629.
- Pax3 cKO, *Nqo1*: Source of variation: variable 1, treatment: p=0.0134; variable 2, PAX3- and PAX3+ MuSC subpopulations: p=0.7403; interaction: p=0.8276.
- Pax3 Ctrl, *Cyp1a2*: Source of variation: variable 1, treatment: p=0.0009; variable 2, PAX3- and PAX3+ MuSC subpopulations: p=0.1051; interaction: p=0.1035.
- Pax3 cKO, *Cyp1a2*: Source of variation: variable 1, treatment: p=0.0006; variable 2, PAX3- and PAX3+ MuSC subpopulations: p=0.8030; interaction: p=0.8061.
- Pax3 Ctrl, *Cyp1b1*: Source of variation: variable 1, treatment: p=0.0001; variable 2, PAX3- and PAX3+ MuSC subpopulations: p=0.1902; interaction: p=0.0071.
- Pax3 cKO, *Cyp1b1*: Source of variation: variable 1, treatment: p=0.0108; variable 2, PAX3- and PAX3+ MuSC subpopulations: p=0.6482; interaction: p=0.0901.

ANOVA was followed by Sidak's post-test. P values between the groups (Vehicle vs. TCDD or between PAX3- and PAX3+ MuSC subpopulations) in Sidak's post-test are shown at the top of the panel (NS, not significant).

Figure 6D: Means \pm SEM (n=3), repeated measure (RM) two-way ANOVA, groups: GFP-vehicle vs GFP- TCDD vs GFP+ vehicle vs GFP+ TCDD. ANOVAs were performed in each mice genotype (Pax3 Ctrl or Pax3 cKO) for each myogenic status (PAX7+/MYOD- or PAX7+/MYOD+). Repeated measure: PAX3- and PAX3+ MuSC subpopulations per conditions. ANOVAs results are detailed below:

- Pax3 Ctrl, PAX7+/MYOD-: Source of variation: variable 1, treatment: p=0.0020; variable 2, PAX3- and PAX3+ MuSC subpopulations: p=0.0102; interaction: p=0.0041.
- Pax3 Ctrl, PAX7+/MYOD+: Source of variation: variable 1, treatment: p=0.0020; variable 2, PAX3- and PAX3+ MuSC subpopulations: p=0.0102; interaction: p=0.0041.
- Pax3 cKO, PAX7+/MYOD-: Source of variation: variable 1, treatment: p=0.0002; variable 2, PAX3- and PAX3+ MuSC subpopulations: p=0.1280; interaction: p=0.7235.
- Pax3 cKO, PAX7+/MYOD+: Source of variation: variable 1, treatment: p=0.0002; variable 2, PAX3- and PAX3+ MuSC subpopulations: p=0.1280; interaction: p=0.7235.

ANOVA was followed by Sidak's post-test. P values between the groups (Vehicle vs. TCDD or between PAX3- and PAX3+ MuSC subpopulations) in Sidak's post-test are shown at the top of the panel (NS, not significant).

Figure 6G: Means \pm SEM (n=5), repeated measure (RM) two-way ANOVA, groups: GFP-vehicle vs GFP- TCDD vs GFP+ vehicle vs GFP+ TCDD. ANOVAs were performed for each localization of AHR (cytoplasmic, both or nuclear). Repeated measure: PAX3- and PAX3+ MuSC subpopulations per conditions. ANOVAs results are detailed below:

- Cytoplasmic: Source of variation: variable 1, treatment: $p < 0.0001$; variable 2, PAX3- and PAX3+ MuSC subpopulations: $p < 0.0001$; interaction: $p < 0.0001$.
- Both cytoplasmic and nuclear: Source of variation: variable 1, treatment: $p = 0.0038$; variable 2, PAX3- and PAX3+ MuSC subpopulations: $p = 0.0077$; interaction: $p < 0.0001$.
- Nuclear: Source of variation: variable 1, treatment: $p < 0.0001$; variable 2, PAX3- and PAX3+ MuSC subpopulations: $p = 0.0014$; interaction: $p = 0.0003$.

ANOVA was followed by Sidak's post-test. P values between the groups (Vehicle vs. TCDD or between PAX3- and PAX3+ MuSC subpopulations) in Sidak's post-test are shown at the top of the panel (NS, not significant).

Figure 7B: Means \pm SEM (n=3 mice and 100 cells per mice), repeated measure (RM) two-way ANOVA, groups: GFP- vehicle vs GFP- TCDD vs GFP+ vehicle vs GFP+ TCDD. Repeated measure: PAX3- and PAX3+ MuSC subpopulations per conditions. Source of variation: variable 1, treatment: $p = 0.0012$; variable 2, MuSC subpopulations: $p < 0.0001$; interaction: $p = 0.0092$. ANOVA was followed by Sidak's post-test. P values between the groups (Vehicle vs. TCDD or between PAX3- and PAX3+ MuSC subpopulations) in Sidak's post-test are shown at the top of the panel (NS, not significant).

Figure 7C: Means \pm SEM (n=3), repeated measure (RM) two-way ANOVA, groups: GFP-vehicle vs GFP- TCDD vs GFP+ vehicle vs GFP+ TCDD. Repeated measure: PAX3- and PAX3+ MuSC subpopulations per conditions. Source of variation: variable 1, time: $p < 0.0001$; variable 2, MuSC subpopulations: $p < 0.0001$; interaction: $p = 0.0016$. ANOVA was followed by Sidak's post-test. For each time, P values between the groups (Vehicle vs. TCDD or between PAX3- and PAX3+ MuSC subpopulations) in Sidak's post-test are shown at the top of the panel (NS, not significant).

Figure 7D: Means \pm SEM (n=6), repeated measure (RM) two-way ANOVA, groups: GFP-vehicle vs GFP- TCDD vs GFP+ vehicle vs GFP+ TCDD. Repeated measure: PAX3- and PAX3+ MuSC subpopulations per conditions. Source of variation: variable 1, treatment: $p < 0.0001$; variable 2, MuSC subpopulations: $p = 0.0140$; interaction: $p = 0.0045$. ANOVA was followed by Sidak's post-test. P values between the groups (Vehicle vs. TCDD or between PAX3- and PAX3+ MuSC subpopulations) in Sidak's post-test are shown at the top of the panel (NS, not significant).

Figure 7F: Means \pm SEM (n=6 for Pax3 Ctrl at 10 weeks, n=3 for Pax3 cKO at 10 weeks, n=4 for Pax3GFP/+ at 14 and 18 weeks), repeated measure (RM) two-way ANOVA, groups: GFP-

vehicle vs GFP- TCDD vs GFP+ vehicle vs GFP+ TCDD. ANOVAs were performed in each mice genotype (Pax3 Ctrl, Pax3 cKO or Pax3GFP/+) for each time (10, 14 or 18 weeks). Repeated measure: PAX3- and PAX3+ MuSC subpopulations per conditions. ANOVAs results are detailed below:

- Pax3 Ctrl, 10 weeks: Source of variation: variable 1, treatment: $p < 0.0001$; variable 2, PAX3- and PAX3+ MuSC subpopulations: $p < 0.0001$; interaction: $p < 0.0001$.
- Pax3 cKO, 10 weeks: Source of variation: variable 1, treatment: $p = 0.2548$; variable 2, PAX3- and PAX3+ MuSC subpopulations: $p = 0.8639$; interaction: $p > 0.9999$.
- Pax3GFP/+, 14 weeks: Source of variation: variable 1, treatment: $p = 0.0018$; variable 2, PAX3- and PAX3+ MuSC subpopulations: $p = 0.0030$; interaction: $p = 0.0027$.
- Pax3GFP/+, 18 weeks: Source of variation: variable 1, treatment: $p = 0.8748$; variable 2, PAX3- and PAX3+ MuSC subpopulations: $p = 0.4126$; interaction: $p = 0.2197$.

ANOVA was followed by Sidak's post-test. P values between the groups (Vehicle vs. TCDD or between PAX3- and PAX3+ MuSC subpopulations) in Sidak's post-test are shown at the top of the panel (NS, not significant).

Figure 7I: Means \pm SEM ($n=3$), repeated measure (RM) two-way ANOVA, groups: Pax3 Ctrl DMSO vs Pax3 Ctrl Rapamycin vs Pax3 cKO DMSO vs Pax3 cKO Rapamycin. Repeated measure: treatment per genotype. ANOVAs were performed in each MuSC subpopulations and results are detailed below:

- GFP-: Source of variation: variable 1, treatment: $p = 0.8758$; variable 2, genotype: $p = 0.3261$; interaction: $p = 0.8001$.
- GFP+: Source of variation: variable 1, treatment: $p = 0.0130$; variable 2, genotype: $p = 0.0015$; interaction: $p = 0.0390$.

ANOVA was followed by Sidak's post-test. P values between the groups (Ctrl vs. cKO or between DMSO and Rapamycin) in Sidak's post-test are shown at the top of the panel (NS, not significant).

Figure 7K: Means \pm SEM ($n=3$), repeated measure (RM) two-way ANOVA, groups: Pax3 Ctrl DMSO vs Pax3 Ctrl Rapamycin vs Pax3 cKO DMSO vs Pax3 cKO Rapamycin. Repeated measure: treatment per genotype. ANOVAs were performed in each MuSC subpopulations and results are detailed below:

- GFP-: Source of variation: variable 1, treatment: $p = 0.8758$; variable 2, genotype: $p = 0.3261$; interaction: $p = 0.8001$.
- GFP+: Source of variation: variable 1, treatment: $p = 0.0341$; variable 2, genotype: $p = 0.0002$; interaction: $p = 0.0078$.

- ANOVA was followed by Sidak's post-test. P values between the groups (Ctrl vs. cKO or between DMSO and Rapamycin) in Sidak's post-test are shown at the top of the panel (NS, not significant).

ANOVA was followed by Sidak's post-test. P values between the groups (Ctrl vs. cKO or between DMSO and Rapamycin) in Sidak's post-test are shown at the top of the panel (NS, not significant).

Figure S2C: Means \pm SEM (n=4), RM two-way ANOVA. Repeat measure: PAX3- and PAX3+ MuSCs per conditions. Source of variation: variable 1, treatment: $p < 0.0001$ (MYOD-/MYOG-, MYOD+/MYOG+), $p = 0.0031$ (MYOD+/MYOG+), $p = 0.0001$ (MYOD-/MYOG+); variable 2, MuSCs subpopulation: $p < 0.0001$ (MYOD-/MYOG-, MYOD+/MYOG-), $p = 0.0010$ (MYOD+/MYOG+), $p = 0.0001$ (MYOD-/MYOG+); interaction: $p < 0.0001$ (MYOD-/MYOG-, MYOD+/MYOG-), $p = 0.0031$ (MYOD+/MYOG+), $p = 0.0001$ (MYOD-/MYOG+). ANOVA was followed by Sidak's post-test. P values between the groups (Vehicle vs. TCDD or between PAX3- and PAX3+ MuSC subpopulations) in Sidak's post-test are shown at the top of the panel (NS, not significant).

Figure S3G: Means \pm SEM (n=4), one-way ANOVA Krustal-Wallis test, groups: AHR Ctrl + vehicle vs AHR Ctrl + TCDD vs AHR cKO + vehicle vs AHR cKO + TCDD. ANOVAs were performed in each myogenic status (PAX7+/MYOD-, PAX7+/MYOD+ or PAX7-/MYOD+) between the groups. For PAX7+/MYOD- and PAX7+/MYOD+: $p < 0.0001$, PAX7-/MYOD+: $p = 0.0022$. ANOVAs were followed by Dunn's post-tests. P values between the groups in Dunn's post-tests are shown at the top of the panel (NS, not significant).

Figure S5C: Means \pm SEM (n=5000 cells per condition), ordinary two-way ANOVA, groups: PAX3- vehicle vs PAX3- TCDD vs PAX3+ vehicle vs PAX3+ TCDD. Source of variation: variable 1, treatment: $p = 0.0025$; variable 2, MuSC subpopulations: $p < 0.0001$; interaction: $p < 0.0001$. ANOVA was followed by Sidak's post-test. P values between the groups (Vehicle vs. TCDD or between PAX3- and PAX3+ MuSC subpopulations) in Sidak's post-test are shown at the top of the panel (NS, not significant).

REFERENCES

Alonso-Martin, S., Aurade, F., Mademtzoglou, D., Rochat, A., Zammit, P.S., and Relaix, F. (2018). SOXF factors regulate murine satellite cell self-renewal and function through inhibition of beta-catenin activity. *Elife* 7.

Baghdadi, M.B., Castel, D., Machado, L., Fukada, S.I., Birk, D.E., Relaix, F., Tajbakhsh, S., and Mourikis, P. (2018). Reciprocal signalling by Notch-Collagen V-CALCR retains muscle stem cells in their niche. *Nature* 557, 714-718.

Bentzinger, C.F., Wang, Y.X., Dumont, N.A., and Rudnicki, M.A. (2013). Cellular dynamics in the muscle satellite cell niche. *EMBO Rep* 14, 1062-1072.

Bismuth, K., and Relaix, F. (2010). Genetic regulation of skeletal muscle development. *Exp Cell Res* 316, 3081-3086.

Bjornson, C.R., Cheung, T.H., Liu, L., Tripathi, P.V., Steeper, K.M., and Rando, T.A. (2012). Notch signaling is necessary to maintain quiescence in adult muscle stem cells. *Stem Cells* 30, 232-242.

Bock, K.W. (2017). From dioxin toxicity to putative physiologic functions of the human Ah receptor in homeostasis of stem/progenitor cells. *Biochem Pharmacol* 123, 1-7.

Borycki, A.G., Li, J., Jin, F., Emerson, C.P., and Epstein, J.A. (1999). Pax3 functions in cell survival and in pax7 regulation. *Development* 126, 1665-1674.

Boutet, S.C., Cheung, T.H., Quach, N.L., Liu, L., Prescott, S.L., Edalati, A., Iori, K., and Rando, T.A. (2012). Alternative polyadenylation mediates microRNA regulation of muscle stem cell function. *Cell Stem Cell* 10, 327-336.

Boutet, S.C., Disatnik, M.H., Chan, L.S., Iori, K., and Rando, T.A. (2007). Regulation of Pax3 by proteasomal degradation of monoubiquitinated protein in skeletal muscle progenitors. *Cell* 130, 349-362.

Calhabeu, F., Hayashi, S., Morgan, J.E., Relaix, F., and Zammit, P.S. (2013). Alveolar rhabdomyosarcoma-associated proteins PAX3/FOXO1A and PAX7/FOXO1A suppress the transcriptional activity of MyoD-target genes in muscle stem cells. *Oncogene* 32, 651-662.

Carrier, F., Chang, C.Y., Duh, J.L., Nebert, D.W., and Puga, A. (1994). Interaction of the regulatory domains of the murine Cyp1a1 gene with two DNA-binding proteins in addition to the Ah receptor and the Ah receptor nuclear translocator (ARNT). *Biochem Pharmacol* 48, 1767-1778.

Chakkalakal, J.V., Jones, K.M., Basson, M.A., and Brack, A.S. (2012). The aged niche disrupts muscle stem cell quiescence. *Nature* 490, 355-360.

Cheung, T.H., and Rando, T.A. (2013). Molecular regulation of stem cell quiescence. *Nat Rev Mol Cell Biol* 14, 329-340.

Collins, C.A. (2006). Satellite cell self-renewal. *Curr Opin Pharmacol* 6, 301-306.

Copeland, N.G., Jenkins, N.A., and Court, D.L. (2001). Recombineering: a powerful new tool for mouse functional genomics. *Nat Rev Genet* 2, 769-779.

Horst, D., Ustanina, S., Sergi, C., Mikuz, G., Juergens, H., Braun, T., and Vorobyov, E. (2006). Comparative expression analysis of Pax3 and Pax7 during mouse myogenesis. *Int J Dev Biol* 50, 47-54.

Katz B., (1961). The terminations of the afferent nerve fibre in the muscle spindle of the frog. *Philos Trans Royal Soc Lond* 243:221-240.

Ko, C.I., Fan, Y., de Gannes, M., Wang, Q., Xia, Y., and Puga, A. (2016). Repression of the Aryl Hydrocarbon Receptor Is Required to Maintain Mitotic Progression and Prevent Loss of Pluripotency of Embryonic Stem Cells. *Stem Cells* 34, 2825-2839.

Koushik, S.V., Chen, H., Wang, J., and Conway, S.J. (2002). Generation of a conditional loxP allele of the Pax3 transcription factor that enables selective deletion of the homeodomain. *Genesis* 32, 114-117.

Kuang, S., Charge, S.B., Seale, P., Huh, M., and Rudnicki, M.A. (2006). Distinct roles for Pax7 and Pax3 in adult regenerative myogenesis. *J Cell Biol* 172, 103-113.

Kuang, S., Kuroda, K., Le Grand, F., and Rudnicki, M.A. (2007). Asymmetric self-renewal and commitment of satellite stem cells in muscle. *Cell* 129, 999-1010.

Lallemand, Y., Luria, V., Haffner-Krausz, R., and Lonai, P. (1998). Maternally expressed PGK-Cre transgene as a tool for early and uniform activation of the Cre site-specific recombinase. *Transgenic Res* 7, 105-112.

Lee, E.C., Yu, D., Martinez de Velasco, J., Tessarollo, L., Swing, D.A., Court, D.L., Jenkins, N.A., and Copeland, N.G. (2001). A highly efficient Escherichia coli-based chromosome engineering system adapted for recombinogenic targeting and subcloning of BAC DNA. *Genomics* 73, 56-65.

Lee, G., Espirito Santo, A.I., Zwingenberger, S., Cai, L., Vogl, T., Feldmann, M., Horwood, N.J., Chan, J.K., and Nanchahal, J. (2018). Fully reduced HMGB1 accelerates the regeneration of multiple tissues by transitioning stem cells to GALert. *Proc Natl Acad Sci U S A* 115, E4463-E4472.

Lepper, C., and Fan, C.M. (2010). Inducible lineage tracing of Pax7-descendant cells reveals embryonic origin of adult satellite cells. *Genesis* 48, 424-436.

Livak, K.J., and Schmittgen, T.D. (2001). Analysis of relative gene expression data using real-time quantitative PCR and the 2^{-ΔΔC_T} Method. *Methods* 25, 402-408.

Ma, Q. (2001). Induction of CYP1A1. The AhR/DRE paradigm: transcription, receptor regulation, and expanding biological roles. *Curr Drug Metab* 2, 149-164.

Machado, L., Esteves de Lima, J., Fabre, O., Proux, C., Legendre, R., Szegedi, A., Varet, H., Ingerslev, L.R., Barres, R., Relaix, F., *et al.* (2017). In Situ Fixation Redefines Quiescence and Early Activation of Skeletal Muscle Stem Cells. *Cell Rep* 21, 1982-1993.

Madisen, L., Zwingman, T.A., Sunkin, S.M., Oh, S.W., Zariwala, H.A., Gu, H., Ng, L.L., Palmiter, R.D., Hawrylycz, M.J., Jones, A.R., *et al.* (2010). A robust and high-throughput Cre reporting and characterization system for the whole mouse brain. *Nat Neurosci* 13, 133-140.

Marlowe, J.L., and Puga, A. (2005). Aryl hydrocarbon receptor, cell cycle regulation, toxicity, and tumorigenesis. *J Cell Biochem* 96, 1174-1184.

- Mauro, A. (1961). Satellite cell of skeletal muscle fibers. *J Biophys Biochem Cytol* 9, 493-495.
- Megeney, L.A., Kablar, B., Garrett, K., Anderson, J.E., and Rudnicki, M.A. (1996). MyoD is required for myogenic stem cell function in adult skeletal muscle. *Genes Dev* 10, 1173-1183.
- Mourikis, P., Sambasivan, R., Castel, D., Rocheteau, P., Bizzarro, V., and Tajbakhsh, S. (2012). A critical requirement for notch signaling in maintenance of the quiescent skeletal muscle stem cell state. *Stem Cells* 30, 243-252.
- Moyle, L.A., and Zammit, P.S. (2014). Isolation, culture and immunostaining of skeletal muscle fibres to study myogenic progression in satellite cells. *Methods Mol Biol* 1210, 63-78.
- Murphy, M.M., Lawson, J.A., Mathew, S.J., Hutcheson, D.A., and Kardon, G. (2011). Satellite cells, connective tissue fibroblasts and their interactions are crucial for muscle regeneration. *Development* 138, 3625-3637.
- Okey, A.B. (2007). An aryl hydrocarbon receptor odyssey to the shores of toxicology: the Deichmann Lecture, International Congress of Toxicology-XI. *Toxicol Sci* 98, 5-38.
- Olguin, H.C., and Pisconti, A. (2012). Marking the tempo for myogenesis: Pax7 and the regulation of muscle stem cell fate decisions. *J Cell Mol Med* 16, 1013-1025.
- Osoegawa, K., Tateno, M., Woon, P.Y., Frengen, E., Mammoser, A.G., Catanese, J.J., Hayashizaki, Y., and de Jong, P.J. (2000). Bacterial artificial chromosome libraries for mouse sequencing and functional analysis. *Genome Res* 10, 116-128.
- Oustanina, S., Hause, G., and Braun, T. (2004). Pax7 directs postnatal renewal and propagation of myogenic satellite cells but not their specification. *EMBO J* 23, 3430-3439.
- Parzefall, W. (2002). Risk assessment of dioxin contamination in human food. *Food Chem Toxicol* 40, 1185-1189.
- Pavlikova, N., Smetana, P., Halada, P., and Kovar, J. (2015). Effect of prolonged exposure to sublethal concentrations of DDT and DDE on protein expression in human pancreatic beta cells. *Environ Res* 142, 257-263.
- Pawlikowski, B., Pulliam, C., Betta, N.D., Kardon, G., and Olwin, B.B. (2015). Pervasive satellite cell contribution to uninjured adult muscle fibers. *Skelet Muscle* 5, 42.
- Relaix, F. (2006). Skeletal muscle progenitor cells: from embryo to adult. *Cell Mol Life Sci* 63, 1221-1225.
- Relaix, F., Montarras, D., Zaffran, S., Gayraud-Morel, B., Rocancourt, D., Tajbakhsh, S., Mansouri, A., Cumano, A., and Buckingham, M. (2006). Pax3 and Pax7 have distinct and overlapping functions in adult muscle progenitor cells. *J Cell Biol* 172, 91-102.
- Relaix, F., Polimeni, M., Rocancourt, D., Ponzetto, C., Schafer, B.W., and Buckingham, M. (2003). The transcriptional activator PAX3-FKHR rescues the defects of Pax3 mutant mice but

induces a myogenic gain-of-function phenotype with ligand-independent activation of Met signaling in vivo. *Genes Dev* 17, 2950-2965.

Relaix, F., Rocancourt, D., Mansouri, A., and Buckingham, M. (2005). A Pax3/Pax7-dependent population of skeletal muscle progenitor cells. *Nature* 435, 948-953.

Rocheteau, P., Gayraud-Morel, B., Siegl-Cachedenier, I., Blasco, M.A., and Tajbakhsh, S. (2012). A subpopulation of adult skeletal muscle stem cells retains all template DNA strands after cell division. *Cell* 148, 112-125.

Rodgers, J.T., King, K.Y., Brett, J.O., Cromie, M.J., Charville, G.W., Maguire, K.K., Brunson, C., Mastey, N., Liu, L., Tsai, C.R., *et al.* (2014). mTORC1 controls the adaptive transition of quiescent stem cells from G0 to G(Alert). *Nature* 510, 393-396.

Rodgers, J.T., Schroeder, M.D., Ma, C., and Rando, T.A. (2017). HGFA Is an Injury-Regulated Systemic Factor that Induces the Transition of Stem Cells into GAlert. *Cell Rep* 19, 479-486.

Sambasivan, R., Gayraud-Morel, B., Dumas, G., Cimper, C., Paisant, S., Kelly, R.G., and Tajbakhsh, S. (2009). Distinct regulatory cascades govern extraocular and pharyngeal arch muscle progenitor cell fates. *Dev Cell* 16, 810-821.

Scaramozza, A., Park, D., Kollu, S., Beerman, I., Xuefeng, S., Rossi, DJ., Lin, CP., Scadden, DT., Crist, C., and Brack, AS. (2019). Lineage tracing reveals a subset of reserve muscle stem cells capable of clonal expansion under stress. **Cell Stem Cell.**

Seale, P., Sabourin, L.A., Girgis-Gabardo, A., Mansouri, A., Gruss, P., and Rudnicki, M.A. (2000). Pax7 is required for the specification of myogenic satellite cells. *Cell* 102, 777-786.

Singh, K.P., Casado, F.L., Opanashuk, L.A., and Gasiewicz, T.A. (2009). The aryl hydrocarbon receptor has a normal function in the regulation of hematopoietic and other stem/progenitor cell populations. *Biochem Pharmacol* 77, 577-587.

Smith, C.K., 2nd, Janney, M.J., and Allen, R.E. (1994). Temporal expression of myogenic regulatory genes during activation, proliferation, and differentiation of rat skeletal muscle satellite cells. *J Cell Physiol* 159, 379-385.

Stantzou, A., Schirwis, E., Swist, S., Alonso-Martin, S., Polydorou, I., Zarrouki, F., Mouisel, E., Beley, C., Julien, A., Le Grand, F., *et al.* (2017). BMP signaling regulates satellite cell-dependent postnatal muscle growth. *Development* 144, 2737-2747.

Tierney, M.T., Stec, M.J., Rulands, S., Simons, B.D., and Sacco, A. (2018). Muscle Stem Cells Exhibit Distinct Clonal Dynamics in Response to Tissue Repair and Homeostatic Aging. *Cell Stem Cell* 22, 119-127 e113.

van den Brink, S.C., Sage, F., Vertesy, A., Spanjaard, B., Peterson-Maduro, J., Baron, C.S., Robin, C., and van Oudenaarden, A. (2017). Single-cell sequencing reveals dissociation-induced gene expression in tissue subpopulations. *Nat Methods* 14, 935-936.

van Velthoven, C.T.J., de Morree, A., Egner, I.M., Brett, J.O., and Rando, T.A. (2017). Transcriptional Profiling of Quiescent Muscle Stem Cells In Vivo. *Cell Rep* *21*, 1994-2004.

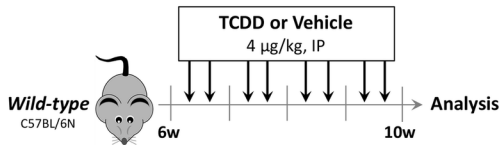
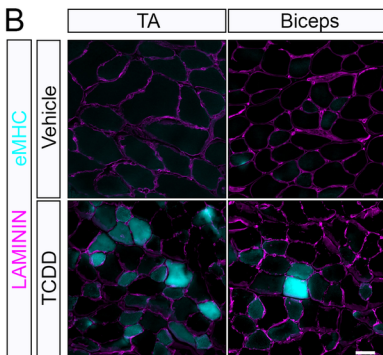
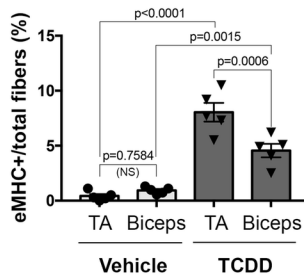
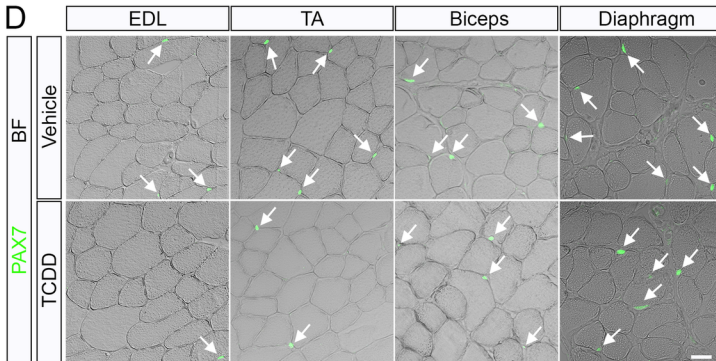
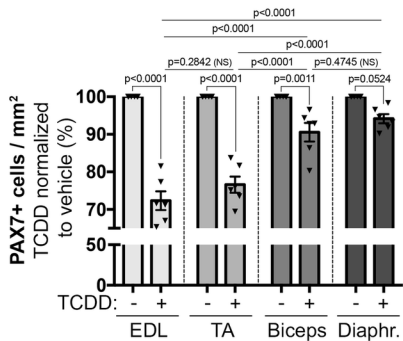
Walisser, J.A., Glover, E., Pande, K., Liss, A.L., and Bradfield, C.A. (2005). Aryl hydrocarbon receptor-dependent liver development and hepatotoxicity are mediated by different cell types. *Proc Natl Acad Sci U S A* *102*, 17858-17863.

Wang, G., Zhu, H., Situ, C., Han, L., Yu, Y., Cheung, T.H., Liu, K., and Wu, Z. (2018). p110alpha of PI3K is necessary and sufficient for quiescence exit in adult muscle satellite cells. *EMBO J* *37*.

Weissman, I.L. (2000). Stem cells: units of development, units of regeneration, and units in evolution. *Cell* *100*, 157-168.

Zammit, P.S., Golding, J.P., Nagata, Y., Hudon, V., Partridge, T.A., and Beauchamp, J.R. (2004). Muscle satellite cells adopt divergent fates: a mechanism for self-renewal? *J Cell Biol* *166*, 347-357.

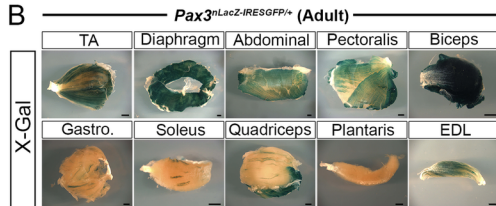
Zammit, P.S., Relaix, F., Nagata, Y., Ruiz, A.P., Collins, C.A., Partridge, T.A., and Beauchamp, J.R. (2006). Pax7 and myogenic progression in skeletal muscle satellite cells. *J Cell Sci* *119*, 1824-1832.

A**B****C****D****E**

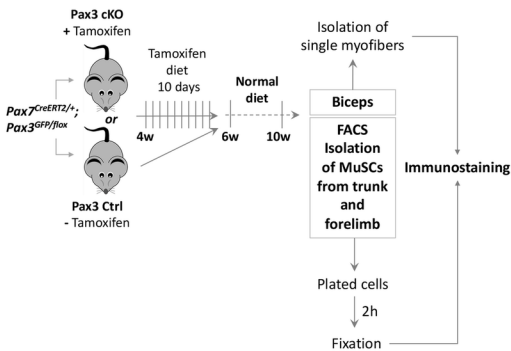
A



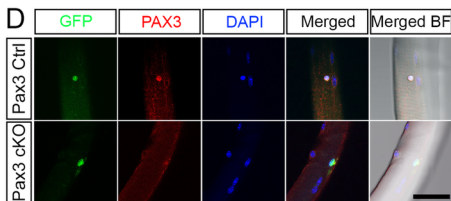
B



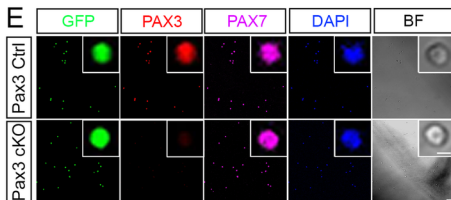
C



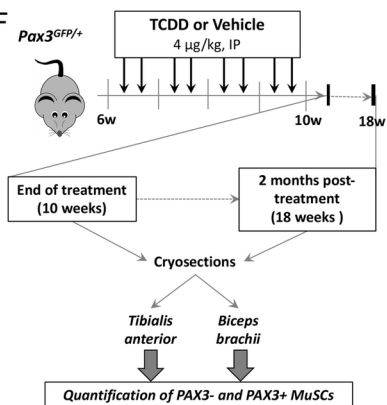
D



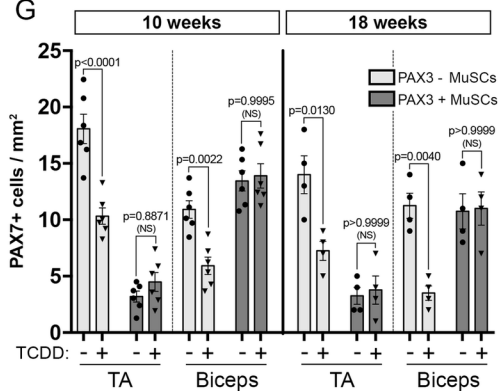
E



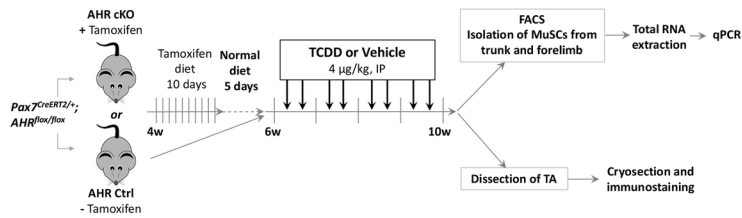
F



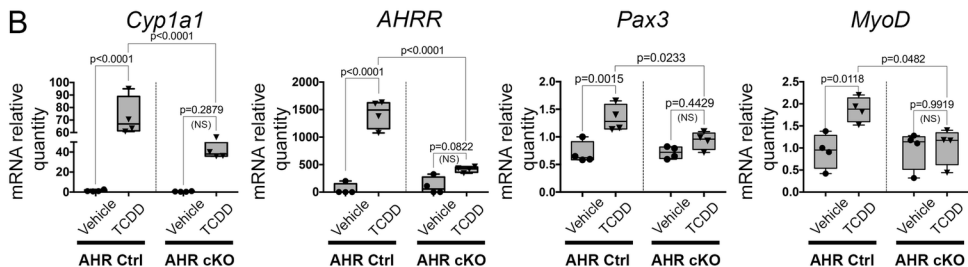
G



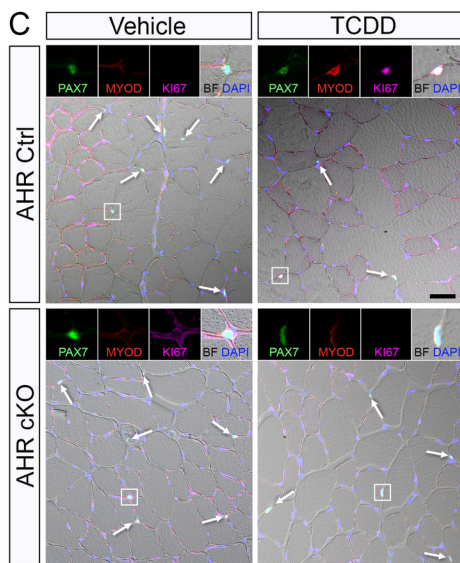
A



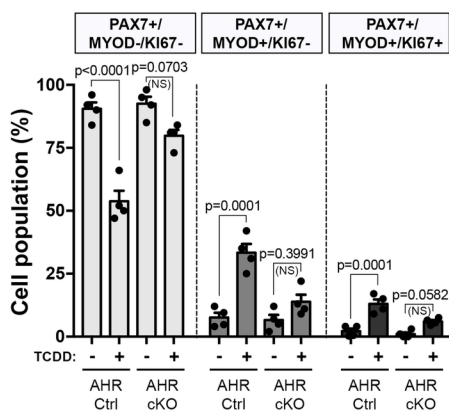
B

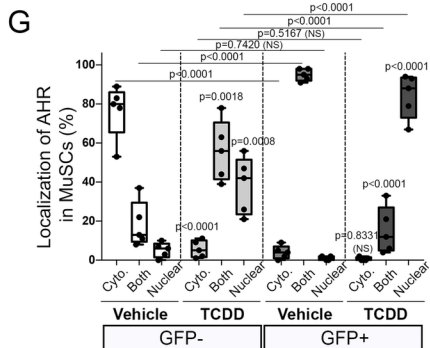
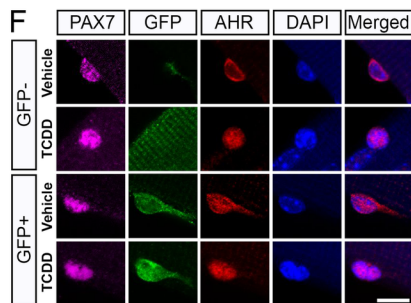
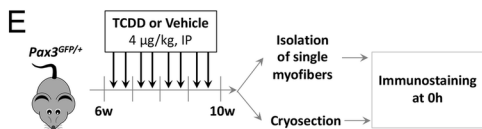
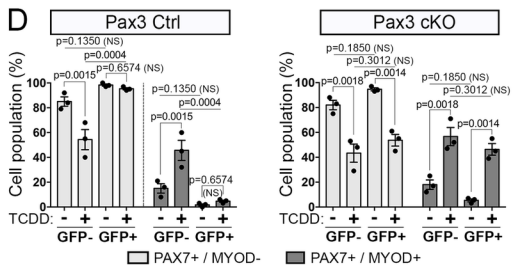
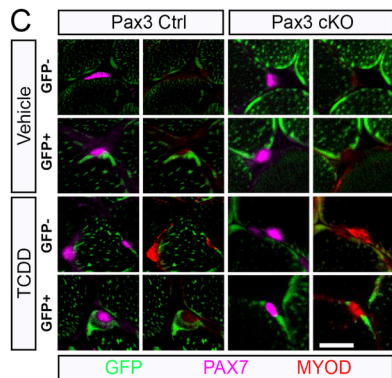
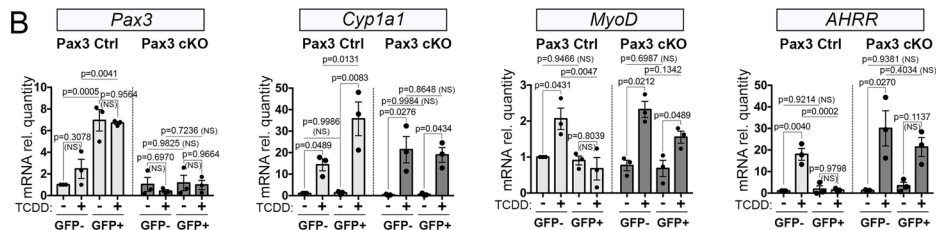
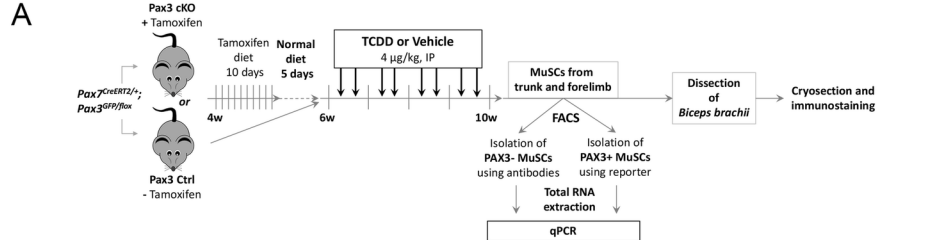


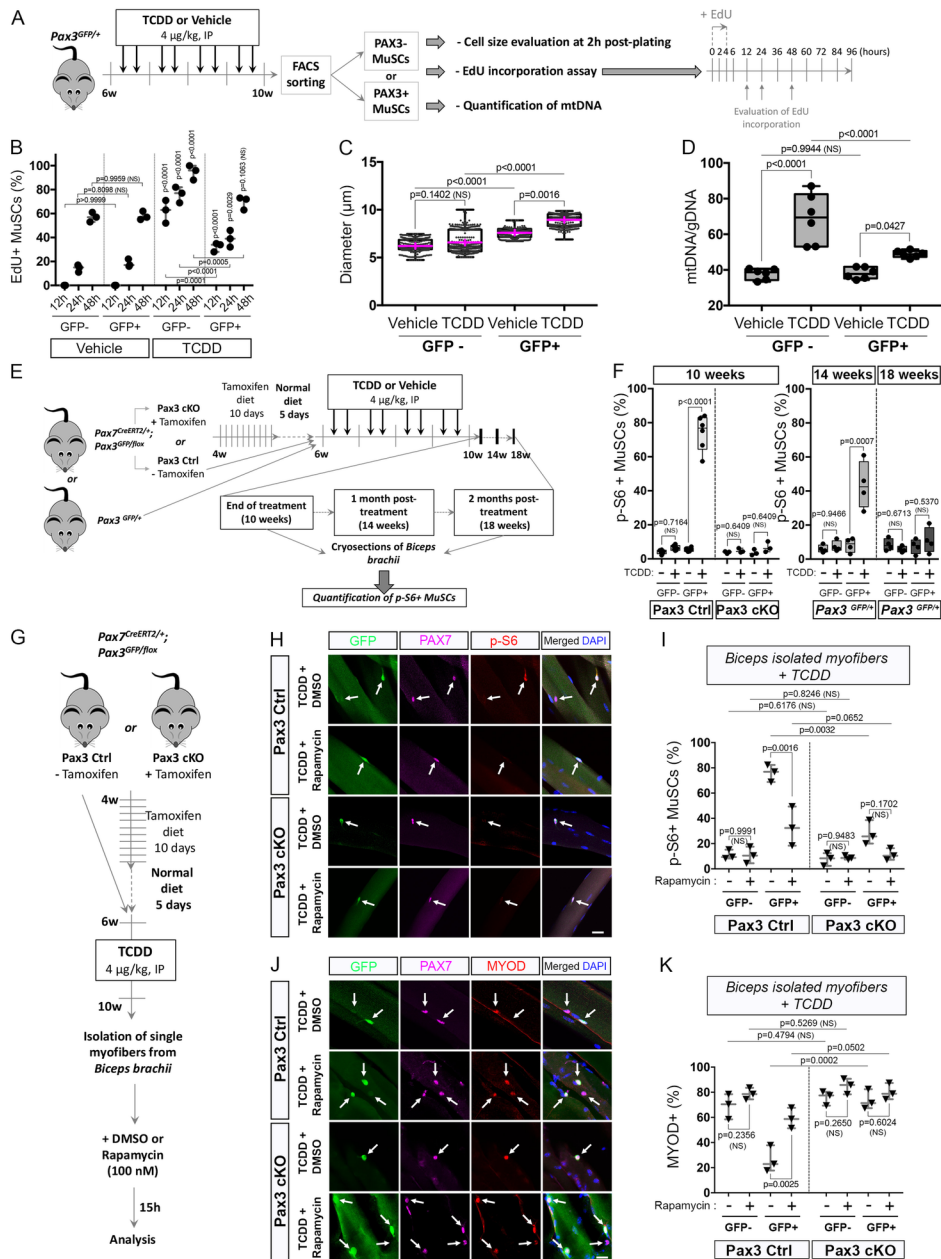
C



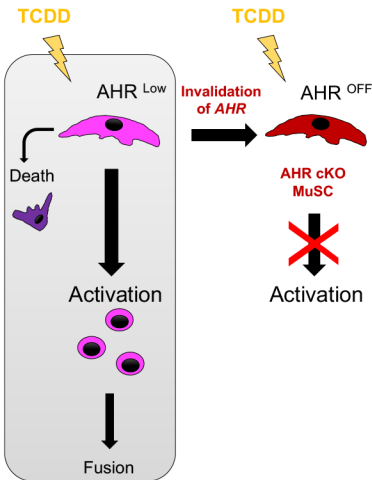
D







PAX3-MuSCs



PAX3+ MuSCs

